

Evolutionary Dynamics Under Various Modes of Reproduction

Jacob Devin Cooper

A dissertation

submitted in partial fulfillment of the
requirements for the degree of

Doctor of Philosophy

University of Washington

2016

Reading Committee:

Benjamin Kerr, Chair

Carl T Bergstrom, Chair

Toby Bradshaw

Program Authorized to Offer Degree:

Biology

©Copyright 2016

Jacob Devin Cooper

University of Washington

Abstract

Evolutionary Dynamics Under Various Modes of Reproduction
Jacob Devin Cooper

Chairs of the Supervisory Committee:
Professor Benjamin Kerr
Professor Carl T Bergstrom
Biology

Chapter 1. Dispersal and migration are spatially limited in many natural populations. Such limitations can lead to clustering of like types, which weakens competition between unlike types; thus, the rate by which a fitter type displaces an inferior competitor can be affected by the spatial scale of movement. We use a birth-death model to show that, by creating competitive refugia, limited migration can increase the frequency of deleterious mutants at mutation-selection balance.

Chapter 2. For a novel genotype to establish in a population, it must (1) be created, and (2) not be subsequently lost. Recombination is a double-edged sword in this process, potentially fostering creation, but also hastening loss as the novel genotype is being recombined with other genotypes, especially when rare. In this chapter, we find that spatial structure may allow a population to harness the creative side of sex while avoiding its destructive side; that is, it may allow a population to create rare genotypes via recombination, and allow those rare genotypes to persist despite recombination.

Chapter 3. In this chapter, we show that classical rules for predicting competitive outcomes in continuous-time systems are appropriate for a certain subset of discrete-time systems, which motivates a new discrete-time competitive exclusion principle. However, in discrete-time systems in which our proof's assumptions are not held, we show that classical rules can fail dramatically.

1
2
3
4
5
6
7
8
9
10
11
12
13
14
15
16
17
18
19
20
21
22
23

Chapter 1

24
25
26
27
28
29
30
31
32
33
34
35
36
37
38
39
40
41
42
43
44
45
46
47
48
49
50
51
52

**Tipping the mutation-selection balance:
Limited migration increases the frequency of deleterious mutants**

Jacob D Cooper^{*,†}, Claudia Neuhauser[‡], Antony M Dean[§], Benjamin Kerr^{*,†}

^{*} *Department of Biology, University of Washington, Seattle, WA*

[†] *BEACON Center for the Study of Evolution in Action, University of Washington, Seattle, WA*

[‡] *Biomedical Informatics and Computational Biology, University of Minnesota, Rochester, MN*

[§] *College of Ecology and Evolution, Sun Yat-sen University, Guangzhou, China*

53 **Running title:**

54 Tipping the Mutation-Selection Balance

55

56 **Corresponding author:**

57 Jacob D Cooper
58 University of Washington
59 Department of Biology
60 Box 351800
61 Seattle, WA 98195-1800

62 phone: (206) 221-7026

63 email: yankel@uw.edu

64

65 **Keywords:**

66 population genetics

67 fitness landscape

68 adaptive valley crossing

69 spatial structure

70 moment closure

71

72

73

74

75

76

77

78 **Abstract:** Typical mutation-selection models assume well-mixed populations, but dispersal and
79 migration within many natural populations is spatially limited. Such limitations can lead to enhanced
80 variation among locations as different types become clustered in different places. Such clustering
81 weakens competition between unlike types relative to competition between like types; thus, the rate by
82 which a fitter type displaces an inferior competitor can be affected by the spatial scale of movement. In
83 this paper, we use a birth-death model to show that limited migration can affect asexual populations by
84 creating competitive refugia. We use a moment closure approach to show that as population structure
85 is introduced by limiting migration, the equilibrium frequency of deleterious mutants increases. We
86 support and extend the model through stochastic simulation, and we use a spatially explicit cellular
87 automaton approach to corroborate the results. We discuss the implications of these results for standing
88 variation in structured populations and adaptive valley crossing in Wright's "shifting balance" process.

89

90

91

92

93

94

95

96

97

98

99

100

101 Most mutations affecting fitness appear to be deleterious (see review by Eyre-Walker and Keightley,
102 2007). A deleterious mutation is expected to persist in a population at a level influenced by the rate at
103 which it is generated and the strength of selection against it. This mutation-selection balance was first
104 developed mathematically by Haldane and Fisher in the 1920's in models that assumed well-mixed
105 populations (Fisher, 1930; Haldane, 1927). However, many natural populations are not well mixed:
106 individuals may not disperse, and even if they do, dispersal or migration is often restricted to nearby
107 locations (Evans et al., 2009; Howells et al., 2013; Martin and Canham, 2010). Such limited movement
108 may influence the proportion of deleterious mutants at equilibrium in several ways. In mating diploid
109 populations, the Wahlund effect (in which population-level heterozygosity is depressed when
110 subpopulations differ in allele frequency) combines with dominance relationships among genotypes to
111 influence the frequency of deleterious mutant alleles (Roze and Rousset, 2004; Whitlock, 2002). In
112 haploid asexual models, limiting migration increases between-deme variation and decreases within-
113 deme variation, but the extent to which this shift in variation affects evolution is unclear.

114 Limitations to migration are not predicted to affect the equilibrium frequency of deleterious
115 mutants in asexual populations when fitness is independent of local composition and density. For
116 instance, Whitlock (2002) finds no effect of migration under a "hard selection" scheme (in which
117 absolute fitness is determined solely by genotype, and thus demes of different compositions may differ
118 in productivity). However, in "soft selection" regimes (in which relative fitness within a deme depends
119 on genotype, but each deme's productivity is the same regardless of composition), demes enriched for
120 mutants are as productive as demes enriched for wild types. Such mutant-rich demes may serve as
121 competitive refugia. Thus, in soft selection schemes, limiting migration can increase the frequencies of
122 deleterious mutants (Roze and Rousset, 2004; Whitlock, 2002).

123 As mutation, selection and migration occur in a subdivided population, both first-order
124 moments (i.e., the mean) and higher-order moments (i.e., variance, skew, kurtosis, etc.) of allele
125 frequencies across demes can change. Previous models have estimated higher-order moments (or
126 related quantities like F_{ST}) in terms of first-order moments under an assumption of weak selection. In
127 this paper, we take a different approach. We build an ecological model of a subdivided population, in
128 which higher-order moments are dynamic variables. No assumptions about the strength of selection or
129 mutation are required. Using this model, we find that limited migration increases the fraction of
130 mutants at mutation-selection balance. However, our moment-closure approach (in which we express
131 third-order moments in terms of lower-order moments) is exact only under total migration. Thus, our
132 analytical results are accurate when there is minimal subdivision. Similar moment closure approaches
133 have been used to model ecological neutrality, competition, and stability (Bolker and Pacala, 1997;
134 Haegeman and Loreau, 2011; Neuhauser, 2002; Vanpeteghem and Haegeman, 2010). We use
135 computer simulations to confirm that the fraction of mutants at equilibrium increases under limited
136 migration (where the mathematical analysis is approximate). The simulations also show spatial
137 segregation of types, suggesting that mutant-rich areas act as competitive refugia.

138

139 **MUTATION-SELECTION BALANCE IN A SUBDIVIDED POPULATION**

140 In our model, a population inhabits a metapopulation of patches. Space is implicit in this model; all
141 patches are equally “far” from any given patch. Migration between patches occurs at birth with a
142 specified probability. When the probability is one, every offspring migrates to a random patch, and the
143 population is essentially well mixed. When the probability is lowered slightly from one, there is a
144 small chance an offspring will stay in its natal patch, and thus a modicum of spatial structure is
145 introduced.

146 **Terminology and Life Cycle:** Consider two genotypes W and M , for wild type and mutant,
147 respectively, inhabiting a metapopulation with an infinite number of patches. The population size of
148 each patch is finite. In all that follows, genotype indices i and j will be used where $i, j \in \{W, M\}$ and
149 $i \neq j$. The per capita birth rate of genotype i is given by $F_i(n_i, n_j) = f_i - \beta_i(n_i + \alpha_{ij}n_j)$, where n_i and
150 n_j are the numbers of genotype i and j in the patch, f_i is the intrinsic growth rate of genotype i , β_i
151 measures the effect of intra-genotypic competition, and α_{ij} is an inter-genotypic conversion factor (i.e.,
152 one individual of genotype j counts as α_{ij} individuals of genotype i). Genotype i dies with rate δ_i .
153 Mutation from genotype i to j occurs during the birth process with probability $\mu_{i \rightarrow j}$. Migration also
154 occurs at birth, when genotype i migrates to a random patch with probability m_i . The population
155 evolves stochastically in continuous time.

156

157 **Moment Dynamics:** Let $N_i(t)$ be the expected number of genotype i per patch at time t . For
158 typographical convenience, we drop the explicit reference to time dependence in our notation for the
159 terms and equations that follow (e.g., $N_i(t)$ is written N_i). In Appendix 1 we show that

$$160 \quad \frac{dN_i}{dt} = (1 - \mu_{i \rightarrow j}) N_i F_i(N_{i|i}, N_{j|i}) + \mu_{j \rightarrow i} N_j F_j(N_{j|j}, N_{i|j}) - \delta_i N_i, \quad (1)$$

161 where $N_{i|j}$ is the expected number of individuals of genotype i in the patch of a randomly chosen
162 individual of genotype j , with $i, j \in \{W, M\}$.

163 It can be shown that $N_{i|i} = N_i + \sigma_i^2/N_i$, where σ_i^2 is the variance in the number of genotype i .

164 When individuals of the given genotype are uniformly distributed (i.e., variance is zero), this reduces

165 to the mean N_i . Similarly, $N_{i|j} = N_i + C/N_j$, where C is the covariance between the numbers of

166 genotypes i and j . When the two genotypes are independently distributed (i.e., covariance is zero) this

167 term reduces to the mean N_i . Covariance may be positive, indicating association between types, or
 168 negative, indicating segregation of types.

169 Thus the dynamics of the first order moments N_i and N_j rely on second order moments σ_i^2 , σ_j^2 ,
 170 and C . The equations governing the dynamics of these second order moments involve third order
 171 moments, the differential equations for the third order moments involve fourth order moments, and so
 172 on. Our task is similar to Hercules' battle with the Hydra (in spirit, not magnitude!). With each Hydra
 173 head Hercules sliced off, new heads popped up in its place. For each moment dynamical equation we
 174 describe, the description of new, higher-order moment equations becomes necessary. We must find a
 175 way to stem the endless flow of higher-order moments. Hercules seared the necks of the Hydra to
 176 prevent the regrowth of the heads; we close our system of differential equations by a second-order
 177 moment closure technique. We approximate third-order moments in terms of lower-order moments
 178 (see Appendix 1 for details), thus sealing the endless flow. Our moment closure approximation is exact
 179 when migration is absolute (i.e., $m_W = m_M = 1$), and we are not limited by assumptions of near
 180 neutrality (Neuhauser, 2002). With this approximation, the dynamics for the second order moments are
 181 given by:

$$\begin{aligned}
 183 \quad \frac{d\sigma_i^2}{dt} = & \frac{dN_i}{dt} + 2\delta_i(N_i - \sigma_i^2) + 2(1 - m_i)(1 - \mu_{i \rightarrow j})\{f_i\sigma_i^2 - \beta_i(N_i + 2N_i\sigma_i^2) - \beta_i\alpha_{ij}(N_iC + N_j\sigma_i^2)\} \\
 184 \quad & + 2(1 - m_j)\mu_{j \rightarrow i}\{f_jC - \beta_j2N_jC - \beta_j\alpha_{ji}(N_iC + N_j\sigma_i^2)\} \quad (2)
 \end{aligned}$$

$$\begin{aligned}
 186 \quad \frac{dC}{dt} = & -(\delta_i + \delta_j)C + (1 - m_i)(1 - \mu_{i \rightarrow j})\{f_iC - \beta_i2N_iC - \beta_i\alpha_{ij}(N_jC + N_i\sigma_j^2)\} \\
 187 \quad & + (1 - m_j)\mu_{j \rightarrow i}\{f_j\sigma_j^2 - \beta_j(N_j + 2N_j\sigma_j^2) - \beta_j\alpha_{ji}(N_jC + N_i\sigma_j^2)\} \\
 188 \quad & + (1 - m_j)(1 - \mu_{j \rightarrow i})\{f_jC - \beta_j2N_jC - \beta_j\alpha_{ji}(N_iC + N_j\sigma_i^2)\} \\
 189 \quad & + (1 - m_i)\mu_{i \rightarrow j}\{f_i\sigma_i^2 - \beta_i(N_i + 2N_i\sigma_i^2) - \beta_i\alpha_{ij}(N_iC + N_j\sigma_i^2)\} \quad (3)
 \end{aligned}$$

190

191 **Mutation-Selection Balance:** Our dynamical system contains many parameters. To simplify matters,
 192 we assume $m_W = m_M = m$, $f_W = f_M = f$, $\beta_W = \beta_M = \beta$, $\alpha_{WM} = \alpha_{MW} = 1$, $\mu_{W \rightarrow M} = \mu$, and
 193 $\mu_{M \rightarrow W} = 0$. Thus, we assume our genotypes are identical in all parameters except their death rates,
 194 which define a W to M mutation as deleterious (i.e. $\delta_M > \delta_W > 0$), and their mutation rates.
 195 Consequently, we only consider viability selection in this analysis, though we simulate other
 196 possibilities below. We have also assumed that intra-genotypic competition is identical to inter-
 197 genotypic competition (the α parameters are set to unity), and that back mutation does not occur. This
 198 might be realistic if the mutation from wild type to the mutant involves a deletion, but even if this
 199 mutation is a base substitution, the density of mutants is often so low that back mutation does not
 200 greatly affect our results (see simulations below).

201 In Appendix 2, we derive the mutant fraction of the population at equilibrium under full
 202 migration ($m = 1$). Because the fraction of mutants cannot be greater than one, there are parameter
 203 constraints on the analysis to ensure mutation does not “overwhelm” selection. Within those parameter
 204 constraints, the fraction of mutants at mutation-selection balance is

$$205 \quad \Phi = \frac{\mu \delta_W}{(1-\mu)(\delta_M - \delta_W)}. \quad (4)$$

206 Like the classical result for a panmictic haploid population, for which $\Phi = \frac{\mu}{s}$ where $1 - s$ is the fitness
 207 of a mutant relative to a wild-type (Crow and Kimura, 1970), our expression is proportional to μ (for
 208 small μ) and inversely proportional to a measure of the selective disadvantage of the mutant ($\frac{\delta_M}{\delta_W} - 1$).

209 How does this fraction change as spatial structure is introduced; that is, what happens to Φ as
 210 m is lowered from unity? Since Equations (2) and (3) are exact for $m = 1$, the partial derivative of Φ
 211 with respect to m can be computed exactly at $m = 1$ (Neuhauser, 2002). In Appendix 3, we derive the
 212 following:

213
$$\left. \frac{\partial \Phi}{\partial m} \right|_{m=1} = - \frac{\beta \mu}{(1-\mu)^2 \delta_M \{(\delta_M / \delta_W)^2 - 1\}} . \quad (5)$$

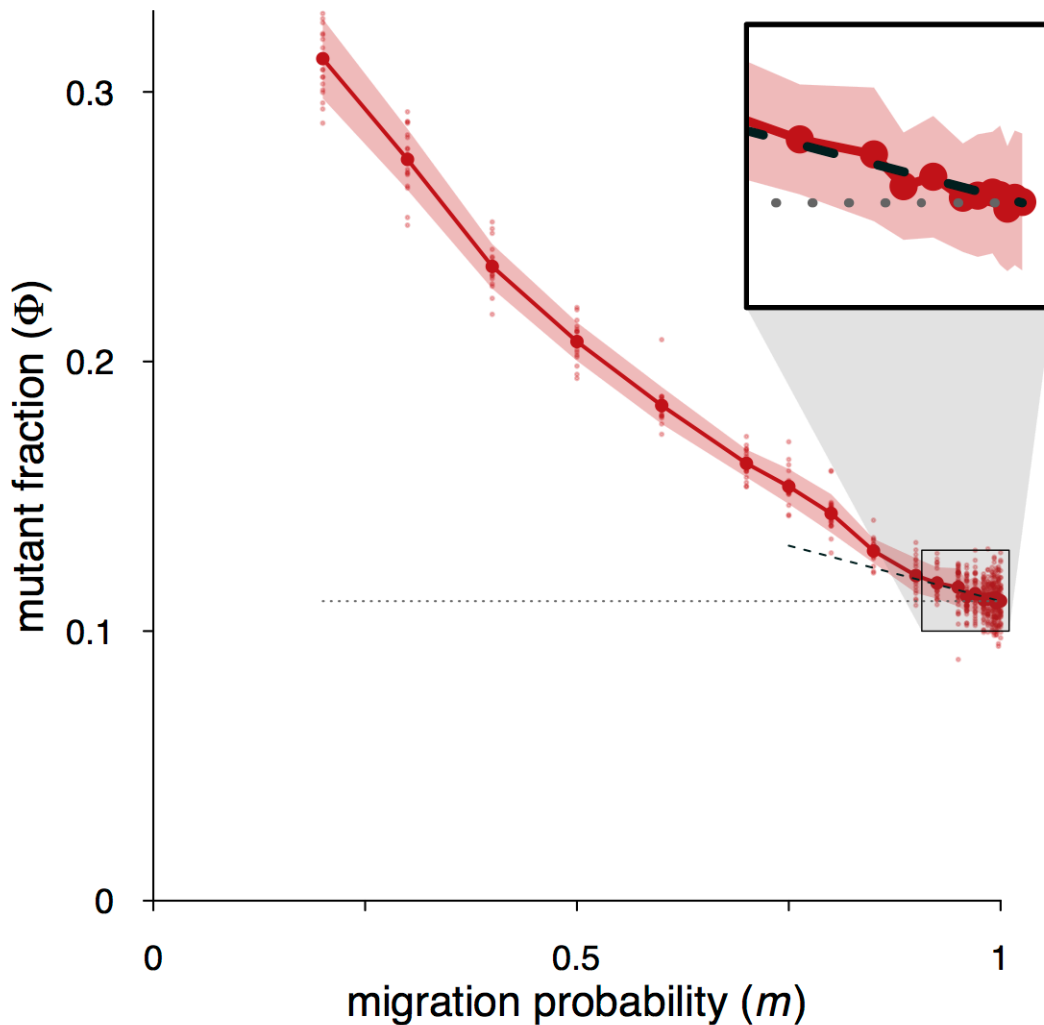
214 This expression demonstrates that $\left. \frac{\partial \Phi}{\partial m} \right|_{m=1} < 0$ for $0 < \mu < 1$, so the fraction of deleterious mutants at
 215 equilibrium always increases when a small amount of structure is introduced into the model.

216

217 **Simulation of the Spatial Model**

218 Our analysis is exact when all offspring migrate, but becomes approximate as soon as some offspring
 219 remain in their natal patches. How well do the approximations capture actual dynamics? Here, we
 220 explore the model via simulation.

221 In the simulation, we seed a finite (but large) number of patches P with wild type and mutant
 222 individuals, and simulate evolution using a Gillespie algorithm in which birth and death events occur
 223 stochastically (see Appendix 4 for details). In simulation runs with absolute migration, all first order
 224 moments and second order moments approach our analytic predictions as equilibrium is reached, even
 225 when initialized far from the calculated equilibrium (Sup. Fig. 1). This is expected, as our analysis is
 226 exact when migration is absolute. As the probability of migration is lowered from unity, our analysis
 227 becomes approximate. Figure 1 shows simulation results across a range of migration probabilities, and
 228 the analytical prediction extrapolated from Equation (5). At high levels of migration, the simulation
 229 corresponds well with the analysis, with Φ following its derivative calculated at $m = 1$ (Fig. 1, inset).
 230 As migration drops further, the mutant frequency rises faster than the linear extrapolation from our
 231 analytical model (Fig. 1). The correspondence between our finite simulation and our deterministic
 232 analysis for high migration indicates that the number of patches P is large enough for the
 233 metapopulation to behave deterministically. Moreover, results are not appreciably affected when fewer
 234 patches are used (Sup. Fig. 2B). Results are also not appreciably affected when back mutation is
 235 allowed (Sup. Fig. 2A).



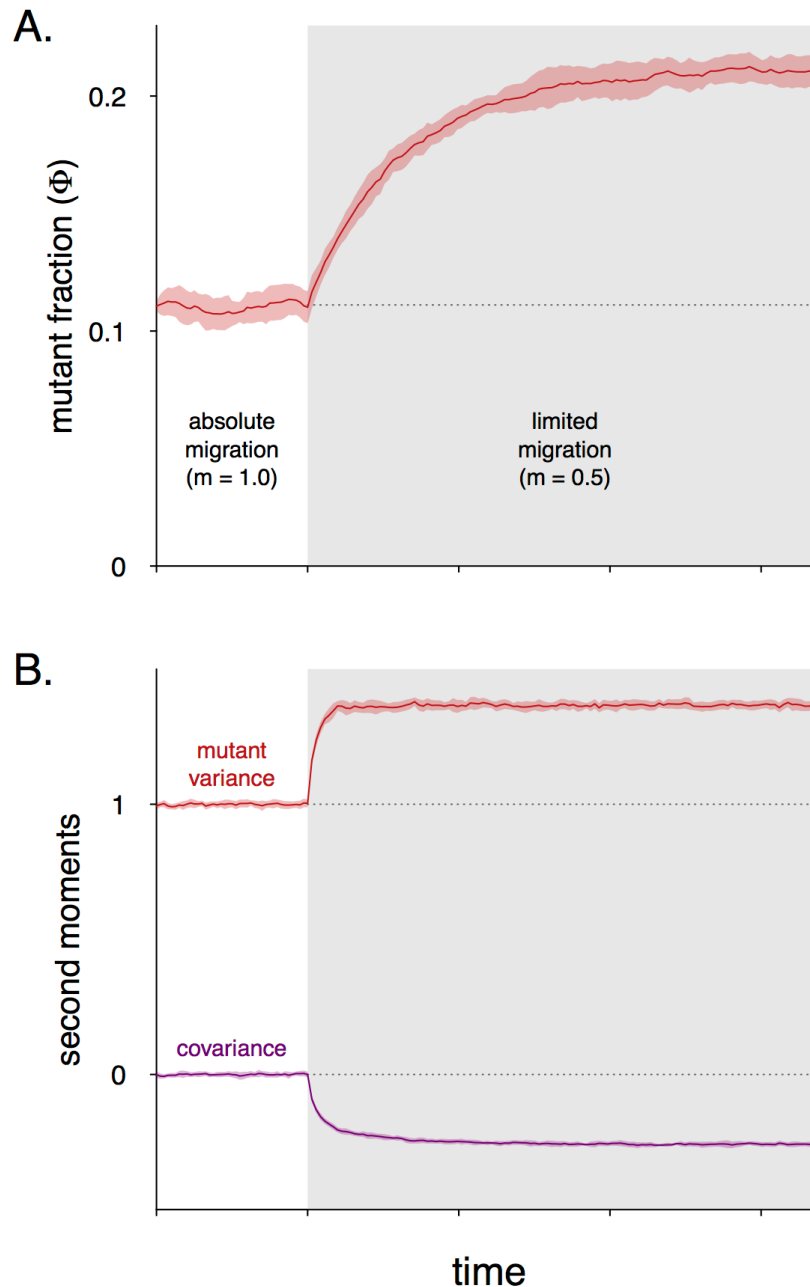
236

237 **Figure 1.** Stochastic simulation under various migration rates. Frequency of deleterious
 238 mutants at mutation-selection balance across various probabilities of migration as found by
 239 simulation (red circles), compared to the $m=1$ derivative of our analytical model (black dashed
 240 line). The analytically calculated mutant fraction at full migration is given as a gray dotted
 241 horizontal line for comparison. At high migration probabilities, the simulation results agree
 242 well with our analytical model (see inset). As the probability of migration decreases further
 243 from unity, the fraction of deleterious mutants increases faster than the analytical
 244 extrapolation. Large data points and shading represent mean values and standard deviation
 245 of 20-40 replicate simulations (small data points) using parameter values $P = 10^4$, $f = 0.5$,
 246 $\beta = 0.2$, $\mu = 0.1$, $\delta_W = 0.05$, $\delta_M = 0.1$, corresponding to a per-patch carrying capacity of
 247 approximately $\frac{f-\delta_W}{\beta} = 2.25$.

248

249 Parameters for Figure 1 were chosen to illustrate a large effect of limited migration on the
250 mutant fraction at mutation-selection balance. When the competition parameter β is decreased,
251 $\text{abs}\left(\frac{\partial\Phi}{\partial m}\Big|_{m=1}\right)$ is proportionately decreased (see Eq. 5) and the per-patch carrying capacity is increased,
252 but the simulated mutant frequency still rises faster than the linear extrapolation from our model (Sup.
253 Fig. 2C). Similar results to those shown in Figure 1 occur when both the mutation rate and the selective
254 disadvantage of mutants are decreased (Sup. Fig. 2D).

255 To see why limited migration increases the fraction of deleterious mutants in a population, we
256 follow a simulation (Fig. 2) as it transitions from absolute migration to limited migration (i.e., $m = 1$
257 to $m = 0.5$). We see that when limited migration is introduced, the mutant frequency increases (Fig.
258 2A), the variance in mutant density increases (i.e., the mutants become more clumped), and the
259 covariance between the densities of the two genotypes becomes negative (i.e., patches with many wild-
260 type genotypes tend to have fewer mutant genotypes, and *vice versa*) (Fig. 2B).



262 **Figure 2.** A simulated shift in the probability of migration. When migration becomes limited
 263 (grey-shaded portion of plots), the increase in deleterious mutant frequency (A) coincides
 264 with an increase in the variance in mutant density and a decrease in the covariance between
 265 mutant and wild type densities (B, variances are divided by the means of their corresponding
 266 variables, and covariance is divided by the product of the roots of the two means). Time units
 267 are relative, and defined by a Gillespie algorithm described in Appendix 4. Solid lines and
 268 colored shading represent the mean \pm SD of 16 replicate simulations using the parameter
 269 values listed in Figure 1.

270 Such spatial segregation leads to an increase in the fraction of inhabited patches that house
271 mutant-only populations (Sup. Fig. 3A). The fraction of mutants in mutant-only patches also increases
272 as the migration rate decreases (Sup. Fig. 3B). Notably, the fraction of mutants in patches that also
273 house wild type genotypes does not increase as the migration rate decreases (Sup. Fig. 3B). Thus, the
274 increase of mutants in mutant-only patches may suffice to explain the overall increase in mutants at
275 limited migration rates.

276 We conclude that limited migration leads to a higher mutant frequency at mutation-selection
277 balance because the less fit mutant is able to escape competition with the wild type due to spatial
278 segregation. Thus, mutant-rich patches are competitive refugia that allow the mutant genotype to
279 persist in relative isolation from the competitively superior wild type. If this explanation is correct,
280 limited migration should safeguard deleterious mutants regardless of whether selection occurs via
281 differences in viability or fecundity, whether space is explicit or implicit, and whether the spatially
282 distributed units are populations or individuals.

283

284

A LATTICE-BASED APPROACH

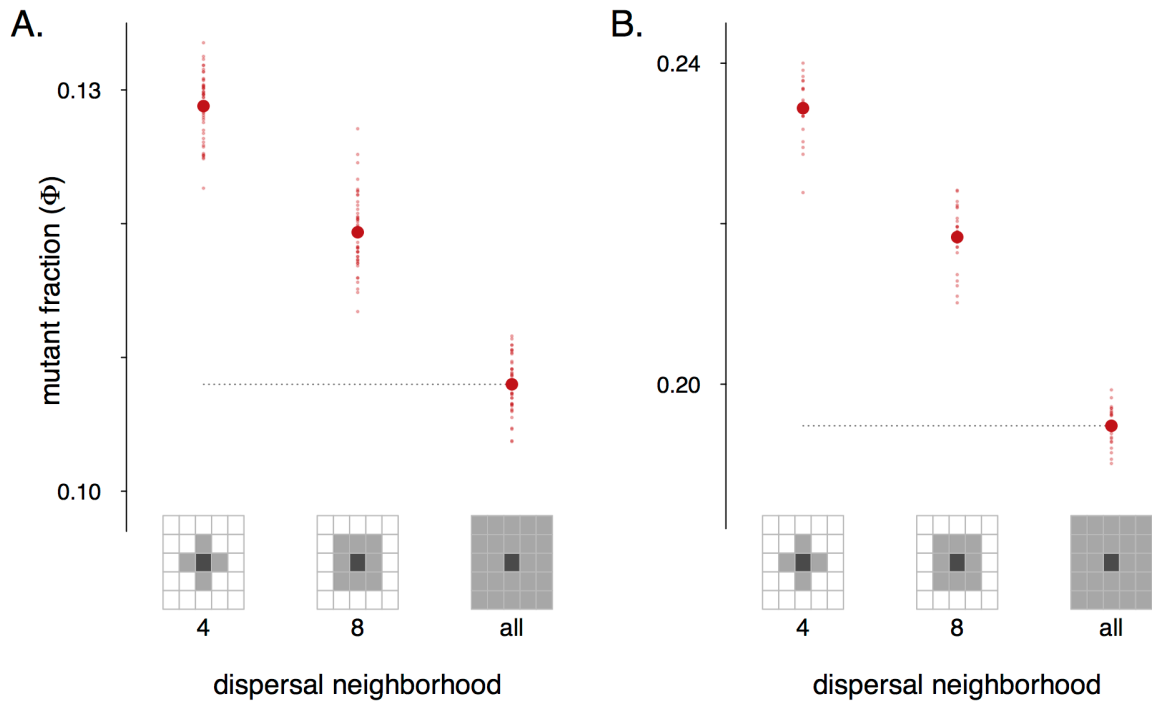
285 Our next approach considers individuals that are embedded in a lattice. Here, unlike our first approach,
286 (a) space is explicit, (b) population structure varies with dispersal distance, (c) the “patches” house
287 individuals rather than subpopulations, and (d) we consider both viability and fecundity selection. A
288 similar lattice-based approach has been used to explore many eco-evolutionary aspects of spatially
289 structured populations, including the invasion of rare types, species coexistence, host-parasite
290 evolution, spatial structuring of communities, and evolutionary trajectories (Débarre et al., 2012;
291 Durrett and Levin, 1997; Hauert and Doebeli, 2004; Kerr et al., 2002).

292 In our simulation, we consider two haploid asexual genotypes: wild type (W) and mutant (M).
293 These genotypes occupy an $L \times L$ regular square lattice with periodic boundaries (i.e., a toroidal
294 geometry). Each lattice point may take one of three states: empty, wild type, or mutant. At each update,
295 a point is chosen at random. If this focal point is “filled” with a wild type, the wild type dies with
296 probability δ_W^* , giving a transformation to the empty state. Likewise, a mutant that is chosen will die
297 with probability δ_M^* (where $\delta_M^* \geq \delta_W^* > 0$).

298 If the focal point is already empty, then a birth event can occur, where an individual in a pre-
299 defined neighborhood of the focal point produces an offspring that fills the focal point (giving a
300 transformation to a filled state). Let x_W and x_M be the fraction of the focal point’s neighborhood
301 occupied by wild type and mutant lattice points, respectively. Then with probabilities $f_W^* x_W$ and $f_M^* x_M$
302 the parent of the individual “born into” the focal point is wild type and mutant, respectively. The
303 parameters f_W^* and f_M^* represent the fecundities of wild-type and mutant individuals (where
304 $0 \leq f_M^* \leq f_W^* \leq 1$). The focal point stays empty with probability $1 - f_W^* x_W - f_M^* x_M$. Mutation occurs
305 at birth: from wild type to mutant with probability $\mu_{W \rightarrow M}^*$, and from mutant to wild type with
306 probability $\mu_{M \rightarrow W}^*$. The degree of population structure is controlled by adjusting the size of the
307 neighborhood around any focal point (effectively altering the distribution of distance at dispersal). We
308 focus on three cases: a von Neumann neighborhood (where the lattice points immediately to the north,
309 east, south and west of the focal point comprise the neighborhood), a Moore neighborhood (where the
310 eight lattice points nearest the focal point constitute the neighborhood), and a Global neighborhood
311 (where the entire lattice, minus the focal point, comprises the neighborhood). Thus, the evolving
312 population can range from highly structured (von Neumann neighborhood) to effectively well mixed
313 (Global neighborhood).

314 Figure 3 shows that smaller dispersal neighborhoods lead to higher mutant frequencies at
 315 equilibrium, corroborating our prior analysis. This pattern holds under both pure viability selection
 316 ($\delta_M^* > \delta_W^*$ and $f_M^* = f_W^*$) and pure fecundity selection ($\delta_M^* = \delta_W^*$ and $f_M^* < f_W^*$).

317
 318
 319
 320
 321
 322



323
 324 **Figure 3.** Lattice-based simulation results. The frequency of deleterious mutants at mutation-
 325 selection balance across various neighborhood sizes in lattice-based simulations with viability
 326 selection (A) or fecundity selection (B). As dispersal is limited to smaller neighborhoods, the
 327 frequency of deleterious mutants increases. Large data points represent mean values of 24
 328 replicate simulations (small data points) using parameter values $L = 200$, $\mu_{W \rightarrow M}^* = 0.1$,
 329 $\mu_{M \rightarrow W}^* = 0.02$, and either viability selection (A, with $\delta_W^* = 0.1$, $\delta_M^* = 0.2$, $f_W^* = f_M^* = 1$) or
 330 fecundity selection (B, with $\delta_W^* = \delta_M^* = 0.1$, $f_W^* = 1$, $f_M^* = 0.5$).

331

DISCUSSION

332

333 We find analytically and computationally that limited migration increases the frequency of deleterious
334 mutants, and this increase is not restricted to a specific form of space or mode of selection. Prior
335 models of selection in metapopulations have shown effects of limited migration when local
336 interactions are defined by mating, or when mutant-rich demes have similar productivity to wild type
337 enriched demes, and can thus act as competitive refugia for mutants (Glémin et al., 2003; Roze and
338 Rousset, 2004; Whitlock, 2002). In this paper, we embedded competition in an explicitly ecological
339 framework, which allows us to manifest local interactions explicitly as density-dependent fecundity.
340 We used a moment closure approach that expresses higher-order moments in terms of lower-order
341 moments, therefore allowing those higher-order moments to vary dynamically as we began to limit
342 migration. We showed that limited migration can affect asexual populations by segregating types.
343 Essentially, limiting migration has no effect on the generation of mutants, but hampers the effective
344 strength of selection (Cherry and Wakeley, 2003) by sheltering alleles from global competition, and so
345 tips the mutation-selection balance in favor of deleterious mutations. Generally, whenever there is both
346 variation in localities and local interaction, migration rate will be a salient factor in determining the
347 frequency of deleterious mutants.

348 Mutant frequency is sometimes used to estimate mutation rates of microbes. Using such a
349 method, a structured environment may appear mutagenic because a higher frequency of mutants is
350 found. For example, Bjedov *et al.* (2003) find a disparity in mutant frequencies between liquid and
351 agar bacterial cultures, and attribute it to oxidative stress incurred during colonial growth on agar. This
352 explanation is certainly plausible, but the colony structure itself may contribute to the increased mutant
353 frequency. When going from an unstructured to a structured environment (e.g., a flask to an agar
354 plate), the frequency of deleterious mutants may increase even if the mutation rate is constant.

355 **Adaptive valley crossing:** If a single deleterious mutation is complemented by a second mutation that
356 improves the fitness of the organism above the wild type, the frequency (and number) of the original
357 mutant may be relevant for crossing “adaptive valleys”. Recent theoretical studies have elucidated how
358 well-mixed populations cross adaptive valleys, and at what rate (Weissman et al., 2010, 2009).
359 However, Sewall Wright’s shifting balance process is predicated on the idea that, collectively, semi-
360 isolated subpopulations would explore a landscape in a way unavailable to well-mixed populations
361 (Pigliucci, 2008; Wright, 1988, 1932). To cross a valley, a population must first discover a new peak,
362 and then have the peak genotype spread through the population. Increasing migration between
363 separated patches hinders exploration of novel genotypes (Whitlock, 2003), but, once a beneficial
364 genotype is discovered, the increased migration facilitates its spread (Jain et al., 2011; Rozen et al.,
365 2008). In the rugged landscapes that were the focus of Wright’s shifting balance, the rate-limiting step
366 in adaptation may be the discovery of novel genotypes (i.e., finding new peaks) rather than their spread
367 through a population. If this is the case, limited migration may speed the rate of adaptation.

368 If valley crossing requires multiple “downward” steps, the facilitating effect of limited
369 migration is amplified. Limited migration protects not only deleterious single mutants from
370 competition with wild types, but also relatively deleterious double mutants from competition with
371 single mutants (and wild types). When deleterious double mutants are added to our metapopulation
372 simulation, we see the amplified effect of limited migration on the double-mutant frequency (Fig. 4A);
373 when we add triple mutants, the effect of limited migration amplifies further (Fig. 4B). This effect on
374 double and triple mutants is also observed in our lattice-based approach (Sup. Fig. 4).

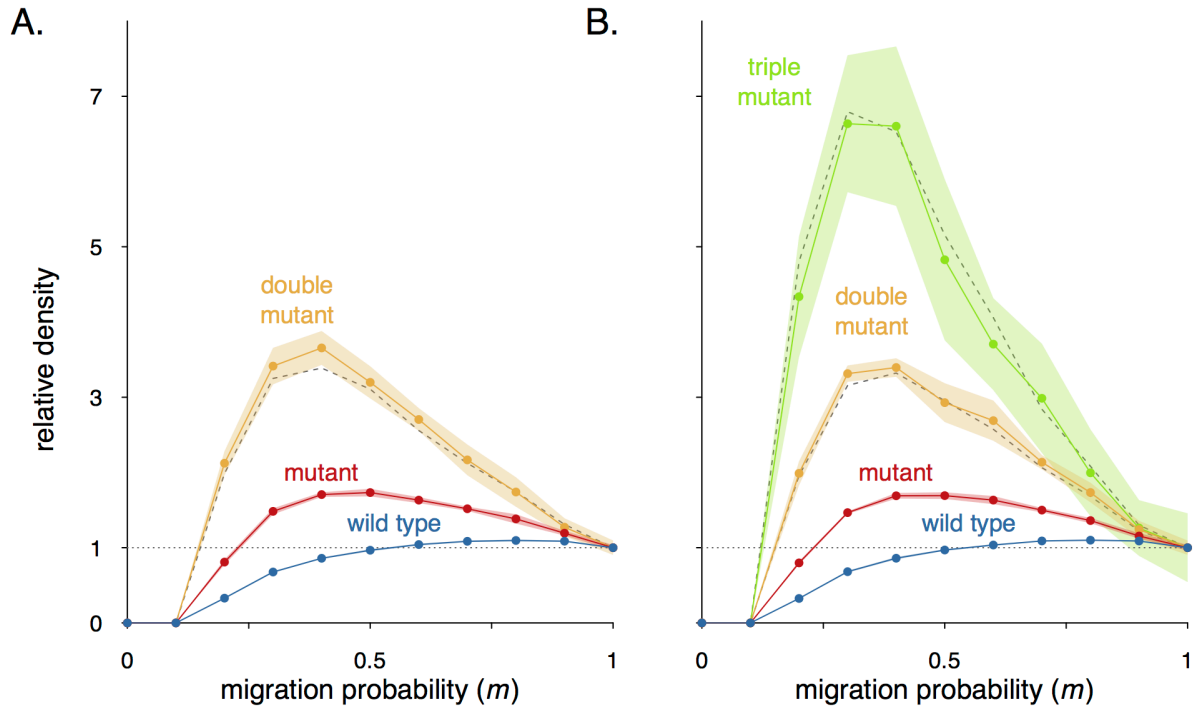
375

376

377

378

379



380 **Figure 4.** Stochastic simulations with a chain of sequential deleterious mutants in a
 381 metapopulation approach. The wild-type genotype yields the first mutant via mutation; the
 382 first mutant yields the relatively deleterious double mutant via mutation; and so on. The
 383 density of each genotype is shown relative to its density in a well-mixed population (given by
 384 the dotted line at unity). The effect of migration probability on relative density in a community
 385 with two (A) and three (B) mutants are shown. Points and colored shading represent the
 386 mean \pm SD of 12 replicate simulations, while dashed lines roughly matching the double-
 387 mutant frequency represent the square of the mutant to wild-type ratio, multiplied by the wild-
 388 type density, for each m . In (B), the cubes of the ratios are also shown, roughly matching the
 389 triple-mutant density. Parameter values used in this simulation are: $P = 10^4$, $f = 0.5$, $\beta = 0.2$,
 390 $\mu_{W \rightarrow M} = \mu_{M \rightarrow M_2} = \mu_{M_2 \rightarrow M_3} = 0.1$, $\mu_{M_3 \rightarrow M_2} = \mu_{M_2 \rightarrow M} = \mu_{M \rightarrow W} = 0.01$, $\delta_W = 0.05$, $\delta_M = 0.1$, $\delta_{M_2} =$
 391 0.2 , $\delta_{M_3} = 0.4$.

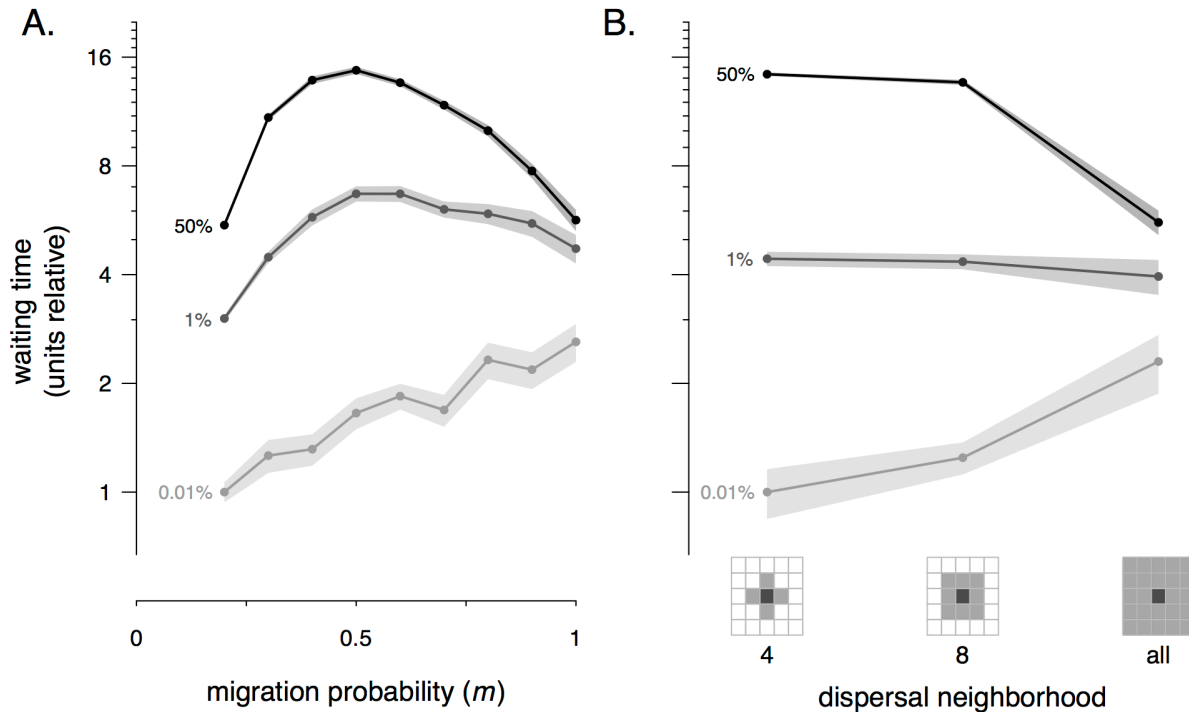
392
393

394 For sufficiently wide valleys, a population starting with only wild type individuals may
 395 discover the peak genotype faster when its migration is limited (Fig. 5). For certain parameter values, a
 396 population whose migration is limited may cross even the narrowest valley—one deleterious mutant
 397 between two peak genotypes—faster than an unstructured population (Bitbol and Schwab, 2014). Note

398 that when only upward steps are required for adaptation (e.g., a smooth landscape) then the rate-
 399 limiting step in adaptation is the spread of beneficial genotypes, and thus limited migration will inhibit
 400 adaptation (Kryazhimskiy et al., 2012).

401

402



403 **Figure 5.** Discovery versus spread in simulated populations. Both metapopulation (A) and
 404 lattice (B) simulations were initialized with wild type genotypes only. There are three
 405 successively more deleterious mutants comprising a valley between the wild type genotype
 406 and a highly beneficial mutant (accessible from the third deleterious mutant). The waiting time
 407 before the beneficial mutant reaches a given frequency is shown. As migration becomes
 408 more limited, the waiting time to the discovery of the beneficial mutant decreases (as m
 409 decreases from 1, the 0.01% profile drops; as the dispersal neighborhood shrinks, the 0.01%
 410 profile drops). However, a greater degree of structure inhibits the spread of these beneficial
 411 mutants (and thus the time to reach a substantial frequency of the beneficial mutant can
 412 increase under initial limitations to migration—see 1% and 50% trajectories). Extremely
 413 limited migration decreases total population size, facilitating spread. Fixation does not occur
 414 as back mutation is allowed and the numbers of patches are large. Points and shaded
 415 regions represent the mean \pm SEM of 24-36 (A) or 16 (B) replicate simulations using
 416 parameter values $f = 0.5$, $\beta = 0.2$, $\mu_{W \rightarrow M} = \mu_{M \rightarrow M2} = \mu_{M2 \rightarrow M3} = 0.1$, $\mu_{M3 \rightarrow M2} = \mu_{M2 \rightarrow M} =$
 417 $\mu_{M \rightarrow W} = 0.01$, $\delta_W = 0.05$, $\delta_M = 0.1$, $\delta_{M2} = 0.2$, $\delta_{M3} = 0.4$, $\delta_{M4} = 0.025$. For (A), $P = 10^4$. For
 418 (B) $L = 200$.

419 The limited migration of individuals generally slows the spread of advantageous traits.
420 However, it is precisely this dampening of competition that can allow spatially structured populations
421 to safeguard deleterious mutants. By harboring this diversity, it may be possible for structured
422 populations to discover novel genotypes faster, even if the benefit spreads more slowly.

423
424
425
426
427
428
429
430
431
432
433
434
435
436
437
438
439
440
441

- 443 Bitbol, A.-F., Schwab, D.J., 2014. Quantifying the Role of Population Subdivision in Evolution on
 444 Rugged Fitness Landscapes. *PLoS Comput Biol* 10, e1003778.
 445 doi:10.1371/journal.pcbi.1003778
- 446 Bjedov, I., Tenaillon, O., Gérard, B., Souza, V., Denamur, E., Radman, M., Taddei, F., Matic, I., 2003.
 447 Stress-induced mutagenesis in bacteria. *Science* 300, 1404–1409. doi:10.1126/science.1082240
- 448 Bolker, B., Pacala, S.W., 1997. Using moment equations to understand stochastically driven spatial
 449 pattern formation in ecological systems. *Theoretical population biology* 52, 179–197.
- 450 Cherry, J.L., Wakeley, J., 2003. A Diffusion Approximation for Selection and Drift in a Subdivided
 451 Population. *Genetics* 163, 421–428.
- 452 Crow, J.F., Kimura, M., 1970. An introduction to population genetics theory.
- 453 Débarre, F., Lion, S., Baalen, Gandon, S., 2012. Evolution of Host Life-History Traits in a Spatially
 454 Structured Host-Parasite System. *The American Naturalist* 179, 52–63. doi:10.1086/663199
- 455 Durrett, R., Levin, S., 1997. Allelopathy in spatially distributed populations. *Journal of Theoretical*
 456 *Biology* 185, 165–171.
- 457 Evans, K.M., Chepurnov, V.A., Sluiman, H.J., Thomas, S.J., Spears, B.M., Mann, D.G., 2009. Highly
 458 Differentiated Populations of the Freshwater Diatom *Sellaphora capitata* Suggest Limited
 459 Dispersal and Opportunities for Allopatric Speciation. *Protist* 160, 386–396.
 460 doi:10.1016/j.protis.2009.02.001
- 461 Eyre-Walker, A., Keightley, P.D., 2007. The distribution of fitness effects of new mutations. *Nat. Rev.*
 462 *Genet.* 8, 610–618. doi:10.1038/nrg2146
- 463 Fisher, R.A., 1930. The Distribution of Gene Ratios for Rare Mutations. *Proc. Roy. Soc. Edinburgh* 50,
 464 205–220.
- 465 Gillespie, D.T., 1977. Exact stochastic simulation of coupled chemical reactions. *J. Phys. Chem.* 81,
 466 2340–2361. doi:10.1021/j100540a008
- 467 Glémin, S., Ronfort, J., Bataillon, T., 2003. Patterns of inbreeding depression and architecture of the
 468 load in subdivided populations. *Genetics* 165, 2193–2212.
- 469 Haegeman, B., Loreau, M., 2011. A mathematical synthesis of niche and neutral theories in
 470 community ecology. *Journal of Theoretical Biology* 269, 150–165.
- 471 Haldane, J.B.S., 1927. A Mathematical Theory of Natural and Artificial Selection, Part V: Selection
 472 and Mutation. *Mathematical Proceedings of the Cambridge Philosophical Society* 23, 838–844.
 473 doi:10.1017/S0305004100015644
- 474 Hauert, C., Doebeli, M., 2004. Spatial structure often inhibits the evolution of cooperation in the
 475 snowdrift game. *Nature* 428, 643–646.
- 476 Howells, E.J., Willis, B.L., Bay, L.K., van Oppen, M.J.H., 2013. Spatial and temporal genetic structure
 477 of *Symbiodinium* populations within a common reef-building coral on the Great Barrier Reef.
 478 *Molecular Ecology* 22, 3693–3708. doi:10.1111/mec.12342
- 479 Jain, K., Krug, J., Park, S.-C., 2011. Evolutionary Advantage of Small Populations on Complex Fitness
 480 Landscapes. *Evolution* 65, 1945–1955. doi:10.1111/j.1558-5646.2011.01280.x
- 481 Kerr, B., Riley, M.A., Feldman, M.W., Bohannan, B.J.M., 2002. Local dispersal promotes biodiversity
 482 in a real-life game of rock-paper-scissors. *Nature* 418, 171–174.
- 483 Kryazhimskiy, S., Rice, D.P., Desai, M.M., 2012. Population Subdivision and Adaptation in Asexual
 484 Populations of *Saccharomyces Cerevisiae*. *Evolution* 66, 1931–1941. doi:10.1111/j.1558-
 485 5646.2012.01569.x

486 Martin, P.H., Canham, C.D., 2010. Dispersal and recruitment limitation in native versus exotic tree
487 species: life-history strategies and Janzen-Connell effects. *Oikos* 119, 807–824.
488 doi:10.1111/j.1600-0706.2009.17941.x

489 Neuhauser, C., 2002. Effects of local interactions and local migration on stability. *Theoretical*
490 *population biology* 62, 297–308.

491 Pacala, S.W., Levin, S.A., 1997. Biologically generated spatial pattern and the coexistence of
492 competing species. *Spatial ecology*. Princeton University Press, Princeton, New Jersey, USA
493 204–232.

494 Pigliucci, M., 2008. Sewall Wright’s adaptive landscapes: 1932 vs. 1988. *Biology and Philosophy* 23,
495 591–603.

496 Roze, D., Rousset, F., 2004. Joint effects of self-fertilization and population structure on mutation load,
497 inbreeding depression and heterosis. *Genetics* 167, 1001–1015.
498 doi:10.1534/genetics.103.025148

499 Rozen, D.E., Habets, M.G.J.L., Handel, A., de Visser, J.A.G.M., 2008. Heterogeneous Adaptive
500 Trajectories of Small Populations on Complex Fitness Landscapes. *PLoS ONE* 3, e1715.
501 doi:10.1371/journal.pone.0001715

502 Vanpeteghem, D., Haegeman, B., 2010. An analytical approach to spatio-temporal dynamics of neutral
503 community models. *Journal of Mathematical Biology* 61, 323–357.

504 Weissman, D.B., Desai, M.M., Fisher, D.S., Feldman, M.W., 2009. The rate at which asexual
505 populations cross fitness valleys. *Theoretical population biology* 75, 286–300.

506 Weissman, D.B., Feldman, M.W., Fisher, D.S., 2010. The rate of fitness-valley crossing in sexual
507 populations. *Genetics* 186, 1389–1410.

508 Whitlock, M.C., 2002. Selection, load and inbreeding depression in a large metapopulation. *Genetics*
509 160, 1191–1202.

510 Whitlock, M.C., 2003. Fixation Probability and Time in Subdivided Populations. *Genetics* 164, 767–
511 779.

512 Wright, S., 1932. The roles of mutation, inbreeding, crossbreeding and selection in evolution, in:
513 *Proceedings of the Sixth International Congress on Genetics*. pp. 356–366.

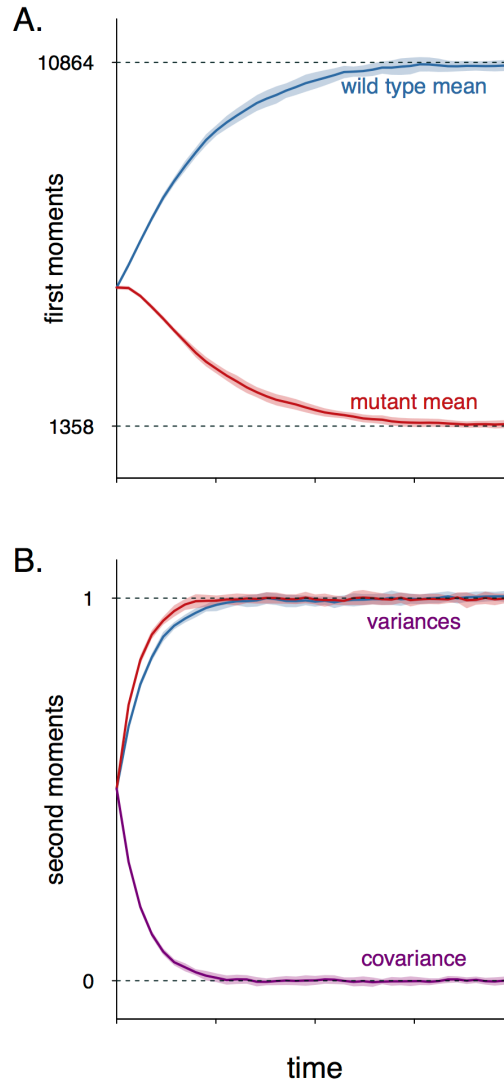
514 Wright, S., 1988. Surfaces of selective value revisited. *The American Naturalist* 131, 115–123.
515
516
517
518
519
520
521
522
523
524
525
526
527
528
529
530
531

532

Supplemental Figures

533

534



535

536

537

538

539

540

541

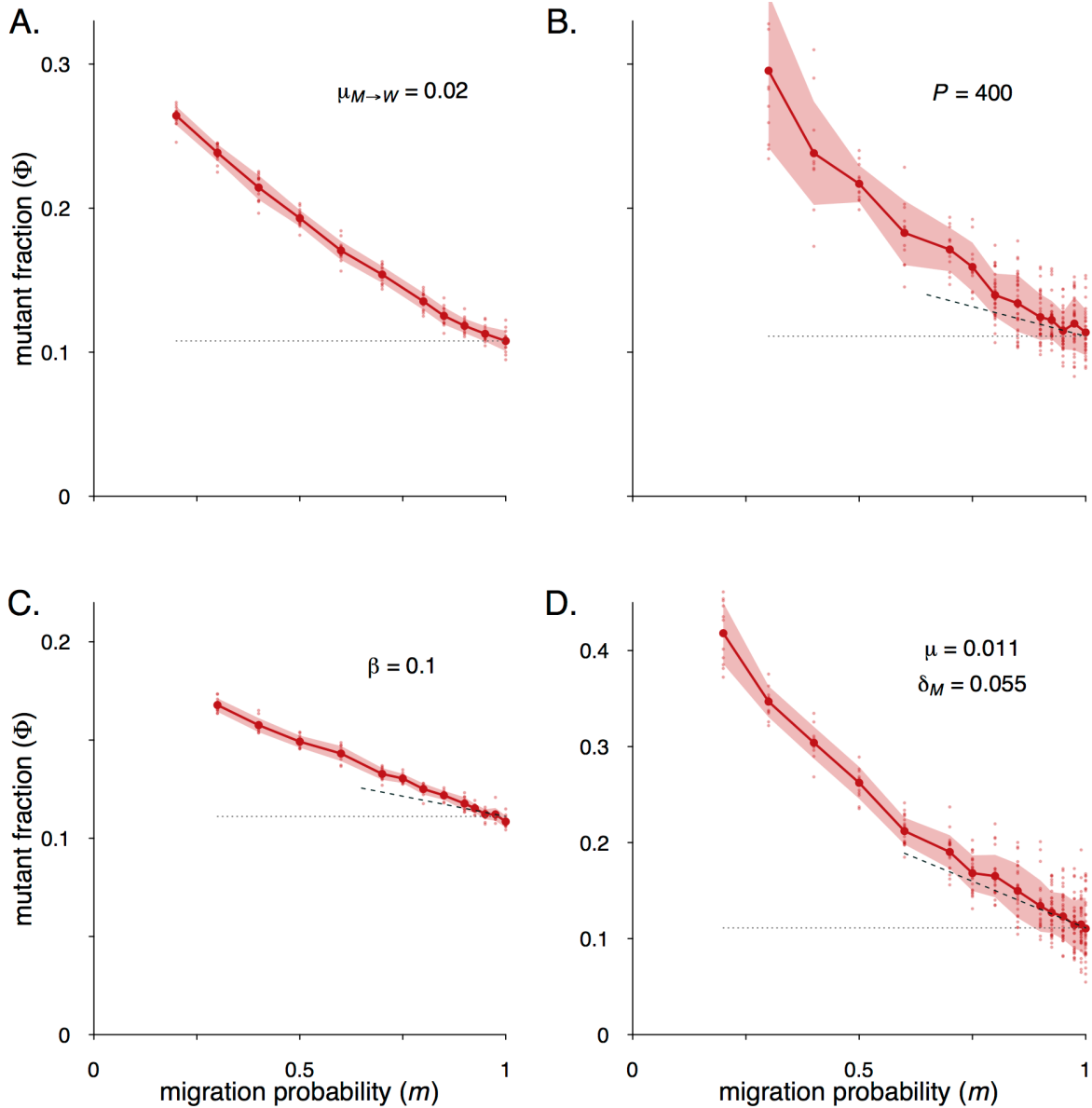
542

543

544

545

Supplemental Figure 1. Stochastic simulation under full migration ($m = 1$). The equilibrium values for all first and second order moments (dashed lines) are calculated from the model. The initial conditions used for the simulation are far removed from these equilibria: each patch starts either empty or with one wild type and one mutant, each with equal probability. All first order moments (A) and second order moments (B) converged to their expected values. In (B), variances are divided by the means of their corresponding variables, and covariance is divided by the product of the roots of the two means. Time units are relative, and defined by a Gillespie algorithm described in Appendix 4. Solid lines and shaded areas represent means \pm SDs of eight replicate simulations using parameter values $P = 10^4$, $f = 0.5$, $\beta = 0.2$, $\mu = 0.1$, $\delta_W = 0.05$, $\delta_M = 0.1$.



546

547

548

549

550

551

552

553

554

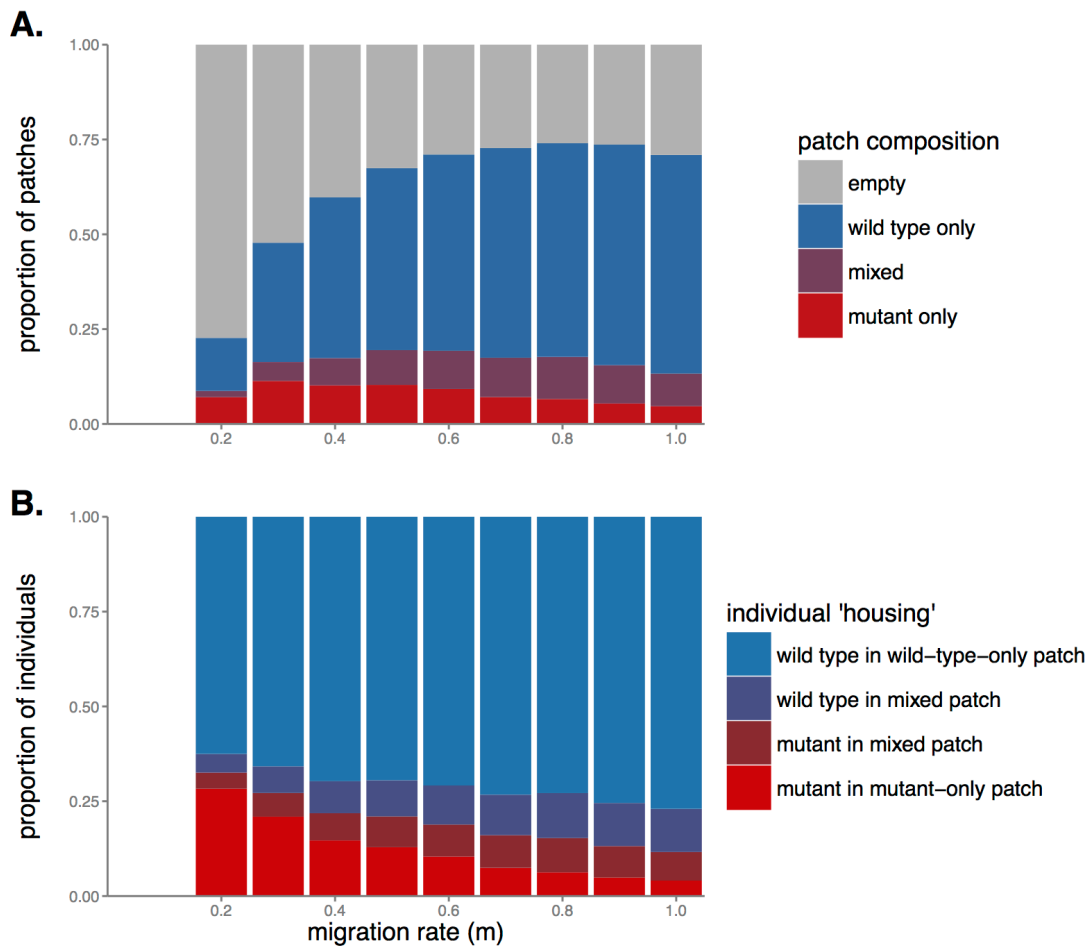
555

556

557

Supplemental Figure 2. Stochastic simulations under various migration rates, with parameters identical to those used for Figure 1 ($P = 10^4$, $f = 0.5$, $\beta = 0.2$, $\mu = 0.1$, $\delta_W = 0.05$, $\delta_M = 0.1$) except with (A) non-zero back mutation rate, (B) fewer patches, (C) decreased competition parameter, and (D) decreased selective disadvantage of mutants with a compensating decrease in mutation rate (see Eq. 4). Frequency of deleterious mutants at mutation-selection balance plotted across various probabilities of migration as found by simulation (red circles), compared to the $m=1$ derivative of our analytical model (black dashed line). The simulated (A) or analytically calculated (B, C, D) mutant fraction at full migration is given as a gray dotted horizontal line for comparison. Large data points and shading represent means \pm SDs of 12-36 replicate simulations (small data points).

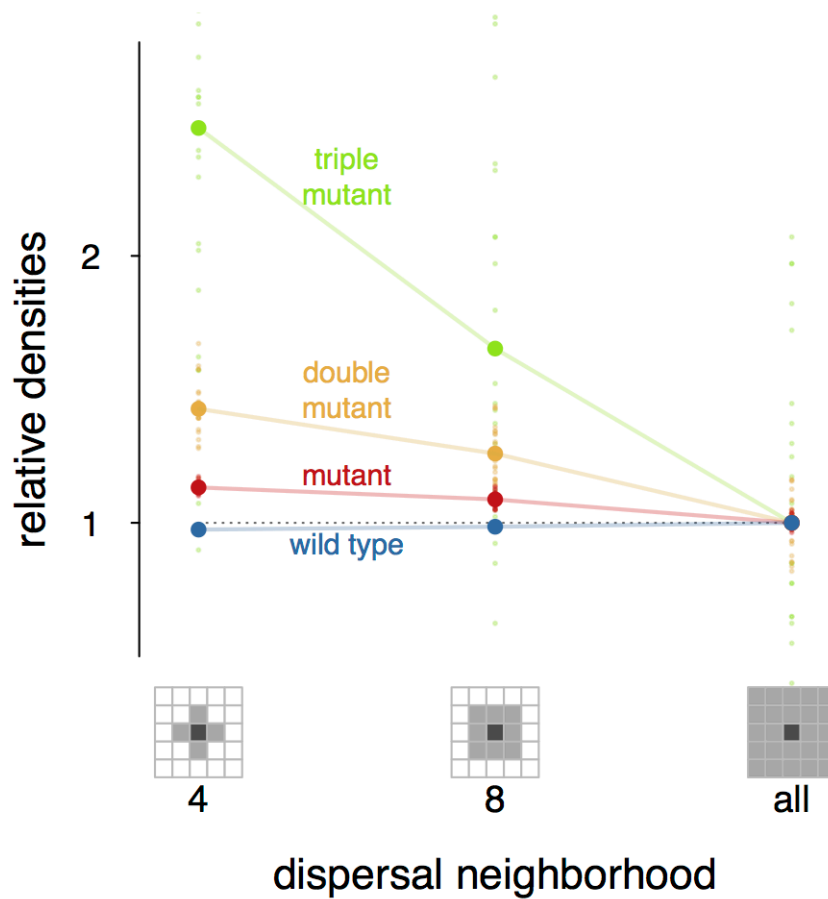
558
559
560
561
562
563
564
565
566
567
568



569
570
571
572
573
574
575
576

Supplemental Figure 3. Patches as competitive refugia for deleterious mutants. The proportion of homotypic, heterotypic, and empty patches at approximately steady-state for a range of migration rates is shown (A). At very low migration rates, the frequency of empty patches increases due to the low rate of reseeding after stochastic within-patch extinctions. The proportion of wild type and mutant individuals 'housed' in homotypic and heterotypic patches is also shown (B). Each bar represents the mean values of two replicate simulations using parameter values $P = 10^4$, $f = 0.5$, $\beta = 0.2$, $\mu = 0.1$, $\delta_W = 0.05$, $\delta_M = 0.1$.

577
 578
 579
 580
 581
 582
 583
 584
 585
 586
 587
 588
 589



590
 591 **Supplemental Figure 4.** Lattice-based simulations with a chain of sequential deleterious
 592 mutants (as in Figure 4). The density of each genotype is shown relative to its density in a
 593 population with a global neighborhood (given by the value of unity). Large data points
 594 represent mean values of 24 replicate simulations (small data points) using parameter values
 595 $L = 200$, $\mu_{W \rightarrow M}^* = \mu_{M \rightarrow M_2}^* = \mu_{M_2 \rightarrow M_3}^* = 0.1$, $\mu_{M_3 \rightarrow M_2}^* = \mu_{M_2 \rightarrow M}^* = \mu_{M \rightarrow W}^* = 0.02$, $\delta_W^* = 0.1$, $\delta_M^* =$
 596 0.2 , $\delta_{M_2}^* = 0.4$, $\delta_{M_3}^* = 0.8$, $f_W^* = f_M^* = f_{M_2}^* = f_{M_3}^* = 1$.

597

Appendices

598 *Appendix 1: Moment Equations*

599 *Mean Density Dynamics*

600 In this appendix, we derive the dynamical equations for our first and second-order moments.
 601 We assume our population inhabits a metapopulation of infinite patches (each of which houses a finite
 602 population), allowing us to use expectation values for our patch dynamics. We start with the dynamics
 603 of the mean genotype abundances. Let $q_i(t)$ be a random variable giving the number of individuals of
 604 genotype $i \in \{W, M\}$ within a randomly selected patch at time t . If we consider a period of time, Δt ,
 605 small enough that the probability of more than one event occurring during that interval is vanishing
 606 small, we have the following:

$$607 \quad q_i(t + \Delta t) = \begin{cases} q_i(t) - 1 & \text{with probability } P_i^- \\ q_i(t) + 1 & \text{with probability } P_i^+ \end{cases}, \quad (\text{A1.1})$$

608 where

$$609 \quad P_i^- = \delta_i q_i(t) \Delta t, \quad (\text{A1.2})$$

610 and

$$611 \quad P_i^+ = (1 - m_i)(1 - \mu_{i \rightarrow j}) F_i(q_i(t), q_j(t)) q_i(t) \Delta t + (1 - m_j) \mu_{j \rightarrow i} F_j(q_j(t), q_i(t)) q_j(t) \Delta t \\ 612 \quad + m_i (1 - \mu_{i \rightarrow j}) E \left[F_i(q_i(t), q_j(t)) q_i(t) \right] \Delta t + m_j \mu_{j \rightarrow i} E \left[F_j(q_j(t), q_i(t)) q_j(t) \right] \Delta t. \quad (\text{A1.3})$$

613 where E is the expectation value over all patches. Thus, the expected change in q_i over our small
 614 interval of time is given by:

$$615 \quad E[\Delta q_i] = E[P_i^+ - P_i^-]. \quad (\text{A1.4})$$

616 For typographical convenience, we drop the explicit time dependence in our notation for the terms and
 617 equations that follow. We use the following notations

$$618 \quad N_i = E[q_i],$$

619
$$\sigma_i^2 = \text{var}[q_i],$$

620
$$C = \text{cov}[q_i, q_j] = \text{cov}[q_j, q_i],$$

621 and we have the following relations

622
$$E[q_i^2] = N_i^2 + \sigma_i^2, \tag{A1.5}$$

623
$$E[q_i q_j] = N_i N_j + C. \tag{A1.6}$$

624 Using (A1.5), (A1.6), and our per capita birth rate of $F_i(n_i, n_j) = f_i - \beta_i(n_i + \alpha_{ij}n_j)$ we can rewrite
625 (A1.4) as follows:

626
$$\frac{E[\Delta q_i]}{\Delta t} = -\delta_i N_i + (1 - \mu_{i \rightarrow j}) \left\{ f_i N_i - \beta_i \left((N_i^2 + \sigma_i^2) + \alpha_{ij} (N_i N_j + C) \right) \right\}$$

627
$$+ \mu_{j \rightarrow i} \left\{ f_j N_j - \beta_j \left((N_j^2 + \sigma_j^2) + \alpha_{ji} (N_i N_j + C) \right) \right\}. \tag{A1.7}$$

628 Taking the limit $\Delta t \rightarrow 0$, and factoring N_i from the second term and N_j from the third term, we have

629
$$\frac{dN_i}{dt} = -\delta_i N_i + (1 - \mu_{i \rightarrow j}) \left\{ f_i - \beta_i \left(\left(N_i + \frac{\sigma_i^2}{N_i} \right) + \alpha_{ij} \left(N_j + \frac{C}{N_i} \right) \right) \right\} N_i$$

630
$$+ \mu_{j \rightarrow i} \left\{ f_j - \beta_j \left(\left(N_j + \frac{\sigma_j^2}{N_j} \right) + \alpha_{ji} \left(N_i + \frac{C}{N_j} \right) \right) \right\} N_j. \tag{A1.8}$$

631 The terms $N_i + \sigma_i^2/N_i$ and $N_j + C/N_i$ (and the two other similar terms) are more approachable if we
632 allow $N_{j|i}$ to represent the expected number of individuals of genotype j in the patch of a randomly
633 chosen individual of genotype i (rather than a randomly chosen patch). Eq. A1.6 can now be rewritten
634 as $N_i N_{j|i} = E[q_i q_j] = N_i N_j + C$, and therefore $N_{j|i} = N_j + C/N_i$. Similarly, Eq. A1.5 yields $N_{i|i} =$
635 $N_i + \sigma_i^2/N_i$. Using this notation, (A1.8) can be simplified to

636
$$\frac{dN_i}{dt} = -\delta_i N_i + (1 - \mu_{i \rightarrow j}) F_i(N_{i|i}, N_{j|i}) N_i + \mu_{j \rightarrow i} F_j(N_{j|j}, N_{i|j}) N_j. \tag{A1.9}$$

637 From these equations we see that change in the first order moment (the expected density of genotype i)
638 depends on second order moments (the variances and covariance of genotype densities). Thus, we now
639 derive the dynamical equations for the change in these second order moments.

640

641 *Variance Dynamics*642 Again, we consider a very small interval of time, Δt . The following holds:

643
$$\Delta q_i^2(t) = q_i^2(t + \Delta t) - q_i^2(t). \quad (\text{A1.10})$$

644 Using (A1.1), (A1.2), (A1.3) and (A1.10), and again dropping the explicit time dependence in our

645 notation, we see that

646
$$\Delta q_i^2 = (q_i - 1)^2 - q_i^2 = -2q_i + 1 \text{ with probability } P_i^-, \text{ and} \quad (\text{A1.11})$$

647
$$\Delta q_i^2 = (q_i + 1)^2 - q_i^2 = 2q_i + 1 \text{ with probability } P_i^+. \quad (\text{A1.12})$$

648 Thus, the expected change in q_i^2 is given by:

649
$$E[\Delta q_i^2] = E[(2q_i + 1)P_i^+ + (-2q_i + 1)P_i^-] \quad (\text{A1.13})$$

650 We have the following relations:

651
$$E[q_i^3] = T_{iii} + 3N_i\sigma_i^2 + N_i^3, \quad (\text{A1.14})$$

652
$$E[q_i^2 q_j] = T_{ijj} + 2N_i C + N_j\sigma_i^2 + N_i^2 N_j, \quad (\text{A1.15})$$

653 where T_{iii} and T_{ijj} are the central third-order moments. Because of (A1.5), we also have

654
$$\frac{E[\Delta q_i^2]}{\Delta t} = \frac{\Delta N_i^2}{\Delta t} + \frac{\Delta \sigma_i^2}{\Delta t} \quad (\text{A1.16})$$

655 Using (A1.5), (A1.6), (A1.14), (A1.15) and (A1.16), taking the limit $\Delta t \rightarrow 0$ and using the chain rule656 (i.e., $\frac{dN_i^2}{dt} = 2N_i \frac{dN_i}{dt}$), we have

657
$$\frac{d\sigma_i^2}{dt} = \frac{dN_i}{dt} + 2(N_i - \sigma_i^2)\delta_i$$
658
$$+ 2(1 - m_i)(1 - \mu_{i \rightarrow j})\{f_i\sigma_i^2 - \beta_i(T_{iii} + 2N_i\sigma_i^2 + \alpha_{ij}(T_{ijj} + N_i C + N_j\sigma_i^2))\}$$
659
$$+ 2(1 - m_j)\mu_{j \rightarrow i}\{f_j C - \beta_j(T_{jji} + 2N_j C + \alpha_{ji}(T_{ijj} + N_i C + N_j\sigma_i^2))\}. \quad (\text{A1.17})$$

660 If we describe the third order moments exactly, we will find ourselves needing to describe fourth order
 661 moments, which will in turn require fifth order moments, and so on. Here we use our moment closure
 662 technique.

663

664 *Closing the Moments*

665 When migration is absolute (i.e., $m_i = m_j = 1$), the random variables q_i and q_j are
 666 independently Poisson distributed among the patches with means equal to N_i and N_j , respectively (see
 667 Neuhauser, 2002). For any independent Poisson-distributed random variables, their third order
 668 moments can be described exactly in terms of lower-order moments; the homogeneous third central
 669 moment is the corresponding first-order moment, while all mixed third central moments are zero:

$$670 \quad T_{iii} = N_i$$

$$671 \quad T_{ijj} = 0$$

672 By using these substitutions as approximations when $m_i \approx m_j \approx 1$, we obviate the need to describe
 673 higher order moments. This moment closure technique is exact when $m_i = m_j = 1$, and approximate
 674 when $m_i \approx m_j \approx 1$.

675 Substituting our approximations for the third central moments into equation (A1.17), we have

$$\begin{aligned}
 676 \quad \frac{d\sigma_i^2}{dt} = & \frac{dN_i}{dt} + 2(N_i - \sigma_i^2)\delta_i \\
 677 & + 2(1 - m_i)(1 - \mu_{i \rightarrow j})\{f_i\sigma_i^2 - \beta_i(N_i + 2N_i\sigma_i^2 + \alpha_{ij}(N_iC + N_j\sigma_i^2))\} \\
 678 & + 2(1 - m_j)\mu_{j \rightarrow i}\{f_jC - \beta_j(2N_jC + \alpha_{ji}(N_iC + N_j\sigma_i^2))\}. \quad (A1.18)
 \end{aligned}$$

679

680

681 *Covariance Dynamics*

682 Again, we consider a very small interval of time, Δt . The following holds:

683
$$\Delta(q_i(t)q_j(t)) = q_i(t + \Delta t)q_j(t + \Delta t) - q_i(t)q_j(t) \quad (\text{A1.19})$$

684 Using, (A1.1), (A1.2), (A1.3) and (A1.16), and again dropping the explicit time dependence in our
685 notations, we see that

686
$$\Delta(q_i q_j) = (q_i - 1)q_j - q_i q_j = -q_j \text{ with probability } P_i^-, \text{ and} \quad (\text{A1.20})$$

687
$$\Delta(q_i q_j) = (q_i + 1)q_j - q_i q_j = q_j \text{ with probability } P_i^+. \quad (\text{A1.21})$$

688 Thus, the expected change in the quantity $q_i q_j$ is:

689
$$E[\Delta(q_i q_j)] = E[-q_j P_i^- - q_i P_j^- + q_j P_i^+ + q_i P_j^+]. \quad (\text{A1.22})$$

690 From (A1.6), we have the following relation:

691
$$\frac{E[\Delta(q_i q_j)]}{\Delta t} = \frac{\Delta(N_i N_j)}{\Delta t} + \frac{\Delta C}{\Delta t}. \quad (\text{A1.23})$$

692 Using (A1.5), (A1.6), (A1.14), (A1.15) and (A1.23), taking the limit $\Delta t \rightarrow 0$, and using the product

693 rule (i.e., $\frac{d(N_i N_j)}{dt} = N_i \frac{dN_j}{dt} + N_j \frac{dN_i}{dt}$), we have

694
$$\begin{aligned} \frac{dC}{dt} = & -(\delta_i + \delta_j)C + (1 - m_i)(1 - \mu_{i \rightarrow j}) \left\{ f_i C - \beta_i \left((T_{iij} + 2N_i C) + \alpha_{ij} (T_{jji} + N_j C + N_i \sigma_j^2) \right) \right\} \\ & + (1 - m_j) \mu_{j \rightarrow i} \left\{ f_j \sigma_j^2 - \beta_j \left((T_{jjj} + 2N_j \sigma_j^2) + \alpha_{ji} (T_{jji} + N_j C + N_i \sigma_j^2) \right) \right\} \\ & + (1 - m_j)(1 - \mu_{j \rightarrow i}) \left\{ f_j C - \beta_j \left((T_{jji} + 2N_j C) + \alpha_{ji} (T_{iij} + N_i C + N_j \sigma_i^2) \right) \right\} \\ & + (1 - m_i) \mu_{i \rightarrow j} \left\{ f_i \sigma_i^2 - \beta_i \left((T_{iii} + 2N_i \sigma_i^2) + \alpha_{ij} (T_{iij} + N_i C + N_j \sigma_i^2) \right) \right\}. \end{aligned}$$

698 Substituting our approximations for the third central moments yields

699
$$\begin{aligned} \frac{dC}{dt} = & -(\delta_i + \delta_j)C + (1 - m_i)(1 - \mu_{i \rightarrow j}) \left\{ f_i C - \beta_i (2N_i C + \alpha_{ij} (N_j C + N_i \sigma_j^2)) \right\} \\ & + (1 - m_j) \mu_{j \rightarrow i} \left\{ f_j \sigma_j^2 - \beta_j ((N_j + 2N_j \sigma_j^2) + \alpha_{ji} (N_j C + N_i \sigma_j^2)) \right\} \\ & + (1 - m_j)(1 - \mu_{j \rightarrow i}) \left\{ f_j C - \beta_j (2N_j C + \alpha_{ji} (N_i C + N_j \sigma_i^2)) \right\} \\ & + (1 - m_i) \mu_{i \rightarrow j} \left\{ f_i \sigma_i^2 - \beta_i ((N_i + 2N_i \sigma_i^2) + \alpha_{ij} (N_i C + N_j \sigma_i^2)) \right\}. \end{aligned} \quad (\text{A1.24})$$

703 With equations (A1.8), (A1.18) and (A1.24), we have a closed system of five differential equations

704 describing the dynamics of N_W , N_M , σ_W^2 , σ_M^2 and C .

705 **Appendix 2: Equilibrium Densities**

706 At equilibrium, $\frac{dN_W}{dt} = \frac{dN_M}{dt} = 0$. In this appendix, we assume $m_W = m_M = m$, $f_W = f_M = f$,

707 $\beta_W = \beta_M = \beta$, $\alpha_{WM} = \alpha_{MW} = 1$, $\mu_{W \rightarrow M} = \mu$ and $\mu_{M \rightarrow W} = 0$. Using these assumptions and equation

708 (A1.8), the equilibrium value \hat{N}_W must satisfy the following:

709
$$0 = -\delta_W \hat{N}_W + (1 - \mu) \{f \hat{N}_W - \beta (\hat{N}_W^2 + \hat{\sigma}_W^2 + \hat{N}_W \hat{N}_M + \hat{C})\}. \quad (\text{A2.1})$$

710 If we assume that $m = 1$, then q_i and q_j are independently Poisson distributed, and therefore:

711
$$\hat{\sigma}_W^2 = \hat{N}_W, \quad (\text{A2.2})$$

712
$$\hat{C} = 0. \quad (\text{A2.3})$$

713 Using (A2.2) and (A2.3), the non-zero equilibrium in (A2.1) is

714
$$\hat{N}_W = \frac{(1-\mu)(f-\beta)-\delta_W}{(1-\mu)\beta} - \hat{N}_M. \quad (\text{A2.4})$$

715 We denote the total density at equilibrium $\hat{T} = \hat{N}_W + \hat{N}_M$. So, we have

716
$$\hat{T} = \frac{(1-\mu)(f-\beta)-\delta_W}{(1-\mu)\beta}, \quad (\text{A2.5})$$

717 and

718
$$\hat{N}_W = \hat{T} - \hat{N}_M. \quad (\text{A2.6})$$

719 Now we turn to the equilibrium density of the mutant genotype, \hat{N}_M , again using (A1.8):

720
$$0 = -\delta_M \hat{N}_M + \{f \hat{N}_M - \beta (\hat{N}_M^2 + \hat{\sigma}_M^2 + \hat{N}_M \hat{N}_W + \hat{C})\} + \mu \{f \hat{N}_W - \beta (\hat{N}_W^2 + \hat{\sigma}_W^2 + \hat{N}_M \hat{N}_W + \hat{C})\}. \quad (\text{A2.7})$$

721 If we are assuming $m = 1$, the resulting Poisson distribution yields

722
$$\hat{\sigma}_M^2 = \hat{N}_M, \quad (\text{A2.8})$$

723 Using (A2.3), (A2.6), and (A2.8), the non-zero mutant equilibrium in (A2.7) is

724
$$\hat{N}_M = \frac{-\mu \hat{T} (f - \beta (\hat{T} + 1))}{-\delta_M + (1 - \mu) (f - \beta (\hat{T} + 1))}. \quad (\text{A2.9})$$

725 After substituting, using (A2.5), and simplifying, equations (A2.4) and (A2.9) simplify to the

726 following:

727
$$\hat{N}_W = \frac{\{(1-\mu)\delta_M - \delta_W\}\{(f-\beta)(1-\mu) - \delta_W\}}{\beta(\delta_M - \delta_W)(1-\mu)^2}, \quad (\text{A2.10})$$

728
$$\hat{N}_M = \frac{\mu\delta_W\{(f-\beta)(1-\mu) - \delta_W\}}{\beta(\delta_M - \delta_W)(1-\mu)^2}. \quad (\text{A2.11})$$

729 In order for \hat{N}_W and \hat{N}_M to be positive, we must have the following two conditions:

730
$$(1 - \mu)(f - \beta) > \delta_W, \quad (\text{A2.12})$$

731
$$(1 - \mu)\delta_M > \delta_W. \quad (\text{A2.13})$$

732 Note that (A2.13) is more stringent than the already assumed $\delta_M > \delta_W$. In all of what follows, we will
 733 assume conditions (A2.12) and (A2.13), except where explicitly mentioned. When $\mu = 0$, equations
 734 (A2.10) and (A2.11) simplify to:

735
$$\hat{N}_W = \frac{f - \beta - \delta_W}{\beta}, \quad \hat{N}_M = 0, \quad (\text{A2.14})$$

736 which gives a positive density of the wild type (by condition (A2.12)) and no mutant density. When
 737 $(1 - \mu)\delta_M = \delta_W$ (i.e., right where equation (A2.13) starts to be violated), equations (A2.10) and
 738 (A2.11) simplify to:

739
$$\hat{N}_W = 0, \quad \hat{N}_M = \frac{f - \beta - \delta_M}{\beta}, \quad (\text{A2.15})$$

740 which gives a positive density of the mutant (by condition (A2.12), replacing δ_W with $(1 - \mu)\delta_M$) and
 741 no wild-type density. Equilibria in (A2.14) and (A2.15) agree with single species equilibria from
 742 ecological models (Neuhauser, 2002; Pacala and Levin, 1997).

743 We let the fraction of mutants in the population be given by $\Phi(t)$, where

744
$$\Phi(t) = \frac{N_M(t)}{N_W(t) + N_M(t)}. \quad (\text{A2.16})$$

745 Using equations (A2.10) and (A2.11), the mutation-selection balance under full migration is:

746
$$\hat{\Phi} = \frac{\mu\delta_W}{(1-\mu)(\delta_M - \delta_W)}. \quad (\text{A2.17})$$

747 Note that if $\mu = 0$, then $\widehat{\Phi} = 0$. That is, when there is no supply of new mutants through mutation,
748 selection “wins” and no mutants remain at equilibrium; this corresponds to the special case of (A2.14).
749 If $\mu = (\delta_M - \delta_W)/\delta_M$, then $\widehat{\Phi} = 1$. That is, as $\mu \rightarrow (\delta_M - \delta_W)/\delta_M$, mutation “wins” by overwhelming
750 selection and only mutants remain at equilibrium; this corresponds to the special case of (A2.15).
751

752 *Appendix 3: The Effect of Structure on Mutation-Selection Balance*

753 In order to explore the role of structure on the mutant frequency, we look at

$$754 \quad \frac{\partial \Phi}{\partial m} = \frac{\frac{\partial N_M}{\partial m} N_W - \frac{\partial N_W}{\partial m} N_M}{(N_W + N_M)^2}. \quad (\text{A3.1})$$

755 Here we will evaluate $\left. \frac{\partial \Phi}{\partial m} \right|_{m=1}$. In order to do so, we must find $\left. \frac{\partial N_W}{\partial m} \right|_{m=1}$ and $\left. \frac{\partial N_M}{\partial m} \right|_{m=1}$, which we
756 abbreviate with $\left. \frac{\partial N_W}{\partial m} \right|_1$ and $\left. \frac{\partial N_M}{\partial m} \right|_1$. To do this we differentiate (A1.8) with respect to m and evaluate at
757 the $m = 1$ equilibrium. We start with equation (A1.8) where $i = W$.

$$758 \quad 0 = \{(1 - \mu)[f - \beta(2\widehat{N}_W + \widehat{N}_M)] - \delta_W\} \left. \frac{\partial N_W}{\partial m} \right|_1 - \{\beta(1 - \mu)\widehat{N}_W\} \left. \frac{\partial N_M}{\partial m} \right|_1 - \{\beta(1 - \mu)\} \left. \frac{\partial \sigma_W^2}{\partial m} \right|_1 - \{\beta(1 - \mu)\} \left. \frac{\partial c}{\partial m} \right|_1. \quad (\text{A3.2})$$

759 Again, we see that we will need to consider partial derivatives of higher-order moments with respect to
760 m to solve (A3.1). By differentiating equations (A1.8) with $i = M$, (A1.18) with $i = W$, (A1.18) with
761 $i = M$, and (A1.24), all with respect to m and making the appropriate substitutions for when $m = 1$,
762 we obtain other equalities involving partial derivatives (similar to (A3.2)). This leads to the following
763 linear system:

$$764 \quad \mathbf{A} \vec{\partial}_1 = \vec{c}, \quad (\text{A3.3})$$

765 where,

$$766 \quad \mathbf{A} = \begin{bmatrix} (1 - \mu)\{f - \beta(2\widehat{N}_W + \widehat{N}_M)\} - \delta_W & -\beta(1 - \mu)\widehat{N}_W & -\beta(1 - \mu) & 0 & -\beta(1 - \mu) \\ -\beta(1 + \mu)\widehat{N}_M + \mu(f - 2\beta\widehat{N}_W) & f - 2\beta\widehat{N}_M - \beta(1 + \mu)\widehat{N}_W - \delta_M & -\beta\mu & -\beta & -\beta(1 + \mu) \\ \delta_W & 0 & -\delta_W & 0 & 0 \\ 0 & \delta_M & 0 & -\delta_M & 0 \\ 0 & 0 & 0 & 0 & -\delta_W - \delta_M \end{bmatrix},$$

767
$$\vec{\partial}_1 = \begin{bmatrix} \left. \frac{\partial N_W}{\partial m} \right|_1 \\ \left. \frac{\partial N_M}{\partial m} \right|_1 \\ \left. \frac{\partial \sigma_W^2}{\partial m} \right|_1 \\ \left. \frac{\partial \sigma_M^2}{\partial m} \right|_1 \\ \left. \frac{\partial C}{\partial m} \right|_1 \end{bmatrix}, \text{ and } \vec{c} = \begin{bmatrix} 0 \\ 0 \\ \widehat{N}_W(1-\mu)\{f - \beta(1 + 2\widehat{N}_W + \widehat{N}_M)\} \\ \widehat{N}_M\{f - \beta(1 + 2\widehat{N}_M + (1+\mu)\widehat{N}_W)\} \\ \widehat{N}_W\{\mu(f - \beta(1 + 2\widehat{N}_W)) - 2\beta\widehat{N}_M\} \end{bmatrix}.$$

768 Solving system (A3.3) and using $\left. \frac{\partial N_W}{\partial m} \right|_1$ and $\left. \frac{\partial N_M}{\partial m} \right|_1$ for equation (A3.1) gives the following:

769
$$\left. \frac{\partial \Phi}{\partial m} \right|_{m=1} = - \frac{\beta\mu}{(1-\mu)^2\delta_M\{(\delta_M/\delta_W)^2-1\}}. \quad (\text{A3.4})$$

770 We abbreviate $\left. \frac{\partial \Phi}{\partial m} \right|_{m=1}$ as $\partial_m \Phi$. From equation (A3.4), it is not difficult to show that $\frac{\partial |\partial_m \Phi|}{\partial \beta} > 0$,

771 $\frac{\partial |\partial_m \Phi|}{\partial \mu} > 0$, $\frac{\partial |\partial_m \Phi|}{\partial \delta_M} < 0$, and $\frac{\partial |\partial_m \Phi|}{\partial \delta_W} > 0$. That is, as the competition coefficient β , the mutation rate μ ,

772 or the death rate of the wild type genotype increase, the addition of structure to an unstructured system
 773 leads to a greater increase in the mutant class frequency. As the death rate of the mutant is increased,
 774 the addition of structure to an unstructured system leads to a smaller increase in the mutant class
 775 frequency.

776

777 **Appendix 4: Gillespie Algorithm**

778 Our simulation is based on a Gillespie algorithm (Gillespie, 1977) that we coded in the Python
 779 2.7 scripting language. The Gillespie algorithm simulates a possible trajectory of a continuous time
 780 stochastic system.

781 In our system of P connected patches, patches must be initialized before simulating evolution.
 782 Unless otherwise indicated, we seeded our patches with wild-type and mutant individuals by
 783 repeatedly drawing from independent Poisson distributions whose parameters are the full migration
 784 equilibria \widehat{N}_W and \widehat{N}_M from (A2.10) and (A2.11), respectively. The initial population defines update

785 zero, for which the time variable t is also zero. As the populations are seeded from their corresponding
 786 $m = 1$ equilibrium distributions, structure is introduced as any limited migration simulation begins.

787 Evolution of the population occurs over “update” steps. First, for update u each patch p
 788 receives four “weights”, corresponding to the four possible events in that patch: a wild-type birth, a
 789 mutant birth, a wild-type death, and a mutant death. Each event’s weight is proportional to its rate. If
 790 we let the number of genotypes W and M in a patch p at update step u be given by $n_W(u, p)$ and
 791 $n_M(u, p)$, respectively, then the weights are defined as follows:

$$792 \quad k_1(u, p) = f n_W(u, p) - \beta n_W(u, p)(n_W(u, p) + n_M(u, p)), \quad (\text{A4.1})$$

$$793 \quad k_2(u, p) = f n_M(u, p) - \beta n_M(u, p)(n_W(u, p) + n_M(u, p)), \quad (\text{A4.2})$$

$$794 \quad k_3(u, p) = \delta_W n_W(u, p), \quad (\text{A4.3})$$

$$795 \quad k_4(u, p) = \delta_M n_M(u, p). \quad (\text{A4.4})$$

796 The event that is attempted at update step u is either a death, a birth with migration, or a birth without
 797 migration, and the decision is made stochastically using the following weights:

$$798 \quad K_{death}(u) = \sum_{p=1}^P k_3(u, p) + \sum_{p=1}^P k_4(u, p), \quad (\text{A4.5})$$

$$799 \quad K_{birth_mig}(u) = m \{ \sum_{p=1}^P k_1(u, p) + \sum_{p=1}^P k_2(u, p) \}, \quad (\text{A4.6})$$

$$800 \quad K_{birth_natal}(u) = (1 - m) \{ \sum_{p=1}^P |k_1(u, p)| + \sum_{p=1}^P |k_2(u, p)| \}. \quad (\text{A4.7})$$

801 Time increment Δt is drawn from an exponential distribution whose rate is equal to $K_{death}(u) +$
 802 $K_{birth_mig}(u) + K_{birth_natal}(u)$, and time parameter t is incremented to $t + \Delta t$. For Figure 2 and
 803 Supplementary Figure 1, the time increment’s exponential distribution rate is equal to $k_1 + k_2 + k_3 +$
 804 k_4 , which does not noticeably affect the resulting time steps.

805 The $K_{birth_natal}(u)$ terms are summed using absolute values due to potentially negative intra-
 806 patch birth rates. Since birth rates decrease linearly with density, $k_1(u, p)$ and $k_2(u, p)$ may be
 807 negative occasionally in particularly crowded patches. For migrating events, the negative births reduce

808 the mean birth rate, which was never negative for the conditions of our simulations. For non-migrating
 809 births, a negative birth event decrements, rather than increments, the chosen genotype population in a
 810 patch. Thus, for any patch r , if a non-migrating birth event is chosen:

$$811 \quad n_W(u + 1, r) = n_W(u, r) + \text{sgn}(k_1(u, r)) \text{ with probability } (1 - \mu) \frac{|k_1(u, r)|}{K_{\text{birth_natal}}(u)}, \quad (\text{A4.8})$$

$$812 \quad n_M(u + 1, r) = n_M(u, r) + \text{sgn}(k_2(u, r)) \text{ with probability } \frac{|k_2(u, r)|}{K_{\text{birth_natal}}(u)} + \mu \frac{|k_1(u, r)|}{K_{\text{birth_natal}}(u)}, \quad (\text{A4.9})$$

813 If a migrating birth event is chosen (i.e., a migrant will ‘land’ on a random patch):

$$814 \quad n_W(u + 1, r) = n_W(u, r) + 1 \text{ with probability } \frac{1-\mu}{P} \sum_{p=1}^P \frac{k_1(u, p)}{K_{\text{birth_mig}}(u)}, \quad (\text{A4.10})$$

$$815 \quad n_M(u + 1, r) = n_M(u, r) + 1 \text{ with probability } \frac{1}{P} \left\{ \sum_{p=1}^P \frac{k_2(u, p)}{K_{\text{birth_mig}}(u)} + \mu \sum_{p=1}^P \frac{k_1(u, p)}{K_{\text{birth_mig}}(u)} \right\}, \quad (\text{A4.11})$$

816 If a death event is chosen:

$$817 \quad n_W(u + 1, r) = n_W(u, r) - 1 \text{ with probability } \frac{k_3(u, r)}{K_{\text{death}}(u)}, \quad (\text{A4.12})$$

$$818 \quad n_M(u + 1, r) = n_M(u, r) - 1 \text{ with probability } \frac{k_4(u, r)}{K_{\text{death}}(u)} \quad (\text{A4.13})$$

819 Simulations were run for 200,000 updates (for $1 \geq m \geq 0.95$), 500,000 updates (for $0.95 > m \geq 0.7$),
 820 or 1,000,000 updates (for $0.7 > m > 0$). Data was recorded every 5000 updates, and equilibril values
 821 represent a simulation’s average state over its final 10,000 updates.

822

823

824

825

826

827

828

Acknowledgements

829

830 The authors thank Michael Whitlock and Ruth Shaw for their helpful comments, and Jacob Speidel,
831 Brian Connelly, and Joshua Nahum for their coding help. The authors are also grateful to the
832 anonymous reviewers for their many useful suggestions. This work was supported in part by the
833 National Science Foundation Graduate Research Fellowship under grants DGE-0718124 and DGE-
834 1256082, as well as NSF Cooperative Agreement DBI-0939454 and an NSF CAREER Award
835 (DEB0952825).

836

837

838

839

840

841

842

843

844

845

846

847

848

849

850

851

852

853

854

855

856

857

858

859

860

861

862

Chapter 2

863

864

865

866

867

868

869

870

871

872

873

874

875

876

877

878

879

880

881

882

Evolution at ‘sutures’ and ‘centers’:

883

Recombination can aid adaptation of spatially structured populations on rugged fitness

884

landscapes

885

886

887

Jacob D Cooper ^{*,†} & Benjamin Kerr ^{*,†}

888

889

890 ^{*} *Department of Biology, University of Washington, Seattle, WA*

891 [†] *BEACON Center for the Study of Evolution in Action, University of Washington, Seattle, WA*

892

893

894

895

896

897

898 **Running title:**

899 Evolution at ‘sutures’ and ‘centers’

900

901 **Corresponding author:**

902 Jacob D Cooper

903 University of Washington

904 Department of Biology

905 Box 351800

906 Seattle, WA 98195-1800

907 phone: (206) 221-7026

908 email: yankel@uw.edu

909

910 **Keywords:**

911 recombination

912 spatial structure

913 rugged fitness landscapes

914 peak-jumping

915

916

917

918

919

920

921 **Abstract:**

922 Epistatic interactions among genes can give rise to rugged fitness landscapes, in which multiple
923 “peaks” of high-fitness allele combinations are separated by “valleys” of low-fitness genotypes. How
924 populations traverse rugged fitness landscapes is a long-standing question in evolutionary biology.
925 Sexual reproduction may affect how a population moves within a rugged fitness landscape. Sex may
926 generate new high-fitness genotypes by recombination, but it may also destroy high-fitness genotypes
927 by shuffling the genes of a fit parent with a genetically distinct mate, creating low-fitness offspring.
928 Either of these opposing aspects of sex require genotypic diversity in the population. Spatially
929 structured populations may harbor more diversity than well-mixed populations, potentially amplifying
930 both positive and negative effects of sex. On the other hand, spatial structure leads to clumping in
931 which mating is more likely to occur between like types, diminishing the effects of recombination. In
932 this study, we use computer simulations to investigate the combined effects of recombination and
933 spatial structure on adaptation in rugged fitness landscapes. We find that spatially restricted mating and
934 offspring dispersal may allow multiple genotypes inhabiting suboptimal peaks to coexist, and
935 recombination at the “sutures” between the clusters of these genotypes can create genetically novel
936 offspring. Sometimes such an offspring genotype inhabits a new peak on the fitness landscape. In such
937 a case, spatially restricted mating allows this fledgling subpopulation to avoid recombination with
938 distinct genotypes, as mates are more likely to be the same genotype. Such population “centers” can
939 allow nascent peaks to establish despite recombination. Spatial structure may therefore allow an
940 evolving population to enjoy the creative side of sexual recombination while avoiding its destructive
941 side.

942

943

944 **Author Summary:**

945 For a novel genotype to establish in a population, it must (1) be created, and (2) not be subsequently
946 lost. Recombination is a double-edged sword in this process, potentially fostering creation, but also
947 hastening loss as the novel genotype is being recombined with other genotypes, especially when rare.
948 In this study, we find that spatial structure may affect both the creative and destructive aspects of
949 recombination in rugged fitness landscapes. By slowing the spread of high-fitness genotypes, spatially
950 restricted mating and dispersal may allow diverse subpopulations to arise. Reproduction across the
951 borders of these subpopulations—at “sutures”—may create genetic novelty. Depending on the
952 topography of the fitness landscape, such novelty may be in the domain of attraction of a new, higher
953 peak; the population may “peak-jump” to an area of genotype space unlikely to be explored by
954 mutation alone. Lineages founded by peak-jumping events are particularly prone to early extinction, as
955 recombination with unlike genotypes may disrupt the rare allele combination and thereby produce low-
956 fitness offspring. However, these fledgling peak lineages may be protected from early extinction by
957 mating within small homotypic clusters—in “centers”. Thus, spatial structure may allow a population
958 to create rare genotypes via recombination, and allow those rare genotypes to persist *despite*
959 recombination.

960

961

962

963

964

965

966

967 **Introduction**

968 Sexual recombination has long been a puzzling evolutionary strategy (see [1,2]). Recombination has
969 the potential to create novel high-fitness genotypes in a population, but also to destroy high-fitness
970 lineages by recombining them with genetically distinct lineages. Whether recombination speeds or
971 slows adaptation depends largely on the relative strengths of its creative and destructive effects.

972

973 One of the earliest adaptive explanations for recombination is the Fisher-Muller effect, in which
974 beneficial alleles in different lineages can recombine into a single lineage, speeding adaptation [3,4].
975 The Fisher-Muller effect exemplifies the creative aspect of sex, and many studies have shown faster
976 adaptation due to Fisher-Muller dynamics [5–8]. However, the Fisher-Muller effect assumes that
977 beneficial alleles remain beneficial when recombined into new genetic backgrounds. This assumption
978 is necessarily broken in multi-peaked fitness landscapes [9], which arise when genetic interactions
979 among loci yield multiple high-fitness allele combinations separated by valleys of low-fitness
980 intermediate genotypes. In such landscapes, the adaptive effects of recombination are more complex.

981

982 Studies on two-locus rugged landscapes focus on escape from suboptimal peaks, and have found that
983 modest levels of recombination may speed adaptation slightly, while substantial recombination slows
984 or halts adaptation entirely [10–12]. However, studies on rugged landscapes with more than two loci
985 yield conflicting results, variously reporting recombination as slowing adaptation [13], speeding
986 adaptation [14], or having complex effects dependent on the topography of a fitness landscape, the
987 population inhabiting it, and the time scale considered [15–17]. Studies on empirical fitness landscapes
988 report recombination as speeding adaptation [6,18] or having complex effects dependent on the fitness
989 topography and rate of recombination [15]. The varied results described above may partly depend on

990 the genetic variation that a particular landscape supports. If there are multiple suboptimal peak
991 genotypes, these competing lineages may interact. Depending on the topography of the fitness
992 landscape, recombination between individuals on different suboptimal peaks may create an offspring
993 in the attractive domain of a novel peak, termed “peak-jumping” [15,19]. Thus, in topographies that
994 permit peak-jumping, when *sub*populations occupy different suboptimal peaks, recombination may
995 allow peak-jumping to novel, higher peaks.

996

997 What conditions might enable a recombining population to maintain the diversity required for peak-
998 jumping? Restricted mating and dispersal (which we call “local reproduction”) may promote
999 population-wide diversity by slowing the spread of high-fitness genotypes and creating competitive
1000 refugia for lower-fitness genotypes [20,21]. However, the same spatial restriction that allows
1001 population-wide diversity also impedes recombination between those diverse types, as mating occurs
1002 largely within monotypic clusters. Martens and Hallatschek [21] show that recombination between
1003 spatially abutting lineages (which we call “sutures”) can be sufficient to speed adaptation due to
1004 Fisher-Muller effects in their smooth landscape model. In some rugged landscapes, recombination at
1005 sutures may allow peak-jumping. However, lineages founded by peak-jumping events are particularly
1006 prone to early extinction as recombination may disrupt the rare allele combinations and consequently
1007 prevent establishment—recombination with the majority genotype may pull fledgling peak populations
1008 off their precipices and into the valley between [22]. On the other hand, recombination within
1009 monotypic clusters (which we call “centers”) may allow high fidelity of rare allele combinations, but
1010 also prevent the creation of such rare allele combinations as no effective recombination is occurring.
1011 Which effects of sutures and centers dominate, and in what circumstances? In this paper, we examine
1012 the combined effects of recombination and local reproduction on adaptation on rugged landscapes.

1013 **Model**

1014 In our simulation, a population inhabits an $L \times L$ regular square lattice with wraparound edges (a
1015 toroid). Each lattice point may be empty or may house one organism. Organisms have a haploid
1016 genotype of N loci, where the allele at each locus is either a 0 or a 1. Each genotype has an associated
1017 survival probability (s_G). Populations are initialized with individuals of the genotype farthest from the
1018 optimal genotype (that is, G_0 such that $H(G_0, G_{opt}) = N$, where H is the Hamming distance operator
1019 and G_{opt} is the optimal genotype), unless otherwise indicated. Evolution occurs via discrete update
1020 steps described below, and simulations conclude when the optimal genotype reaches a predefined
1021 frequency, or when a predefined number of epochs have occurred, where an epoch is defined as $L \times L$
1022 updates.

1023

1024 At each update, a point is chosen at random. If this focal point houses an individual of genotype G , the
1025 individual dies with probability $1 - s_G$, and the lattice point becomes empty. If the focal point is
1026 already empty, then a birth event can occur. For a birth event, two parents are needed. The first parent
1027 is chosen from a pre-defined dispersal neighborhood about the focal point, and second parent is chosen
1028 from a pre-defined mating neighborhood about the first parent. For simplicity, we set the sizes of these
1029 two neighborhoods equal, and call the radius of this neighborhood the “reproductive distance”. We
1030 focus on two extreme cases. In our “local reproduction” condition, a focal point’s neighborhood is
1031 defined by the lattice points immediately to the north, east, south and west (the Von Neumann
1032 neighborhood); in our “global reproduction” condition, the neighborhood is defined as the entire
1033 lattice, minus the focal point.

1034

1035 Once the parents are chosen, an offspring genotype is formed by recombination and mutation. To
1036 simulate recombination, one of the two parents is chosen at random to contribute the allele at the first
1037 locus, and between-locus crossover occurs with probability r . Thus $r = 0$ yields no crossing over,
1038 while $r = 0.5$ yields independent assortment of parental alleles. To simulate mutation, each locus of
1039 the recombined offspring's binary genotype changes its allelic state ($0 \rightarrow 1$ or $1 \rightarrow 0$) with probability μ .
1040 Finally, the offspring is born, and inhabits the initially-empty lattice point.

1041

1042 **Results and Discussion**

1043 To investigate the interplay of recombination and reproductive distance, we use a 4x2 factorial design:
1044 four recombination probabilities and two neighborhood sizes. For each factorial combination, we
1045 simulate replicate populations evolving on a multi-peaked rugged landscape. Our default fitness
1046 landscape is defined to allow peak-jumping; that is, there exist two suboptimal peaks (0011 and 1100)
1047 which can recombine to produce the optimal genotype (1111). We will relax this contrivance later in
1048 our results. In our 4x2 experiment, all populations are initialized on a suboptimal peak (0000), and all
1049 parameters (lattice size, initial density, mutation rate, *etc.*) are held constant for all simulations. We
1050 find that the qualitative effect of recombination – whether it speeds or slows the traversal of the rugged
1051 fitness landscape – can depend on whether reproduction is localized (Figure 1), and this interaction
1052 between recombination and reproductive neighborhood is significant ($p < 0.001$, Manly's permutation
1053 test [23]). When reproduction is global, recombination never speeds, and can even slow, peak
1054 establishment. Conversely, when reproduction is local, recombination never slows but can speed peak
1055 establishment.

1056

1057

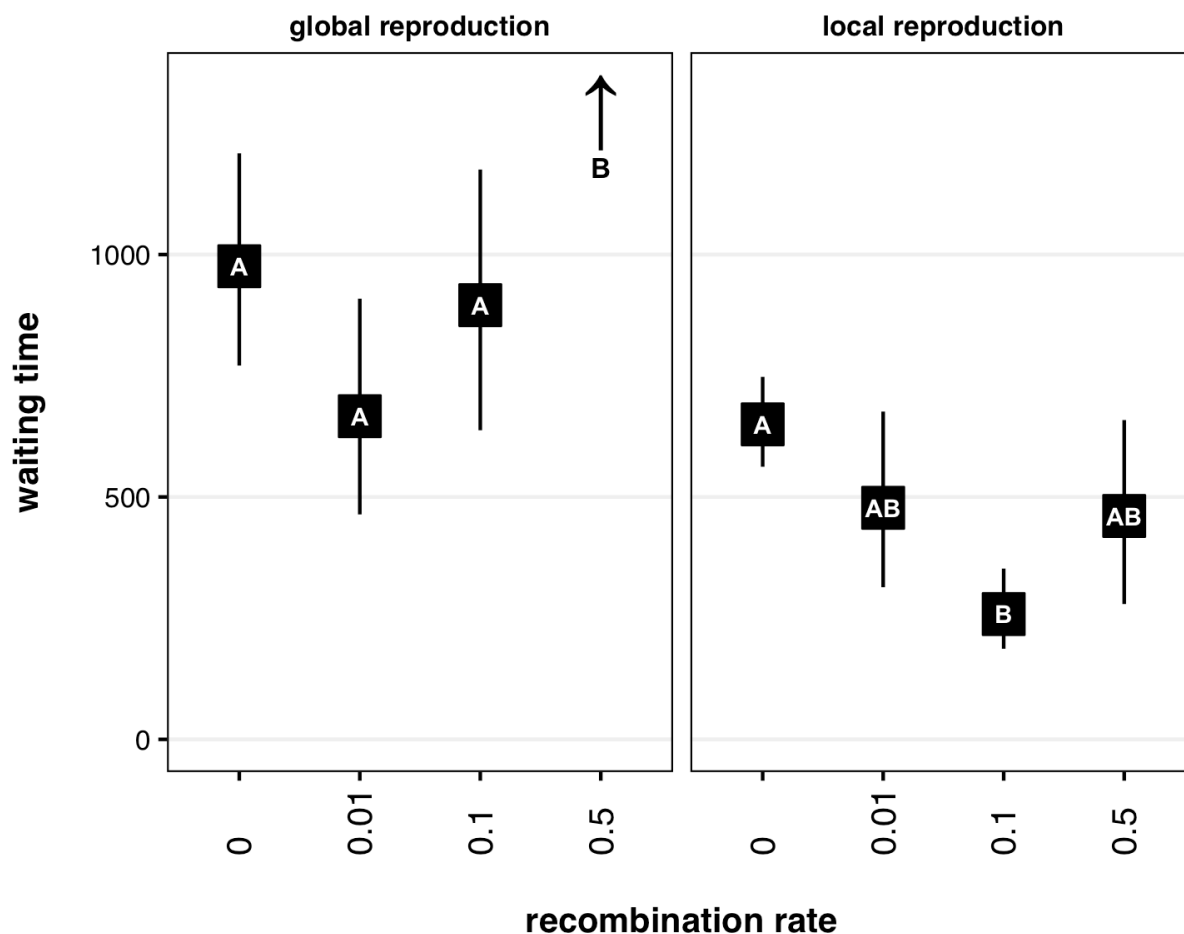
1058

1059

1060

1061

1062



1063

1064

1065

1066

1067

1068

1069

1070

1071

Figure 1. Waiting time to establishment of an optimal peak genotype at various recombination rates. We define establishment as discovery without subsequent extinction, and time as simulation epochs (see Methods). Data points and error bars represent mean values and standard error of 75 replicate simulations using parameter values $L = 70$, $\mu = 0.002$, $s_G = 0.2$, $s_{0000} = 0.6$, $s_{1100} = s_{0011} = 0.85$, $s_{1111} = 0.9$, where G represents all non-specified genotypes. Within each reproductive distance, data points with no shared letter are significantly different (Tukey's HSD, $\alpha = 0.05$). The upward arrow indicates that establishment never occurred by the simulation maximum of 2000 epochs.

1072 To investigate why the effect of recombination may depend on reproductive distance, we focus on two
1073 aspects of a genotype's spread through a population: discovery and establishment. For a peak genotype
1074 to establish in a population, it must (1) be created, and (2) not be subsequently lost.

1075

1076 **Local reproduction fosters the creation of novel genotypes via recombination**

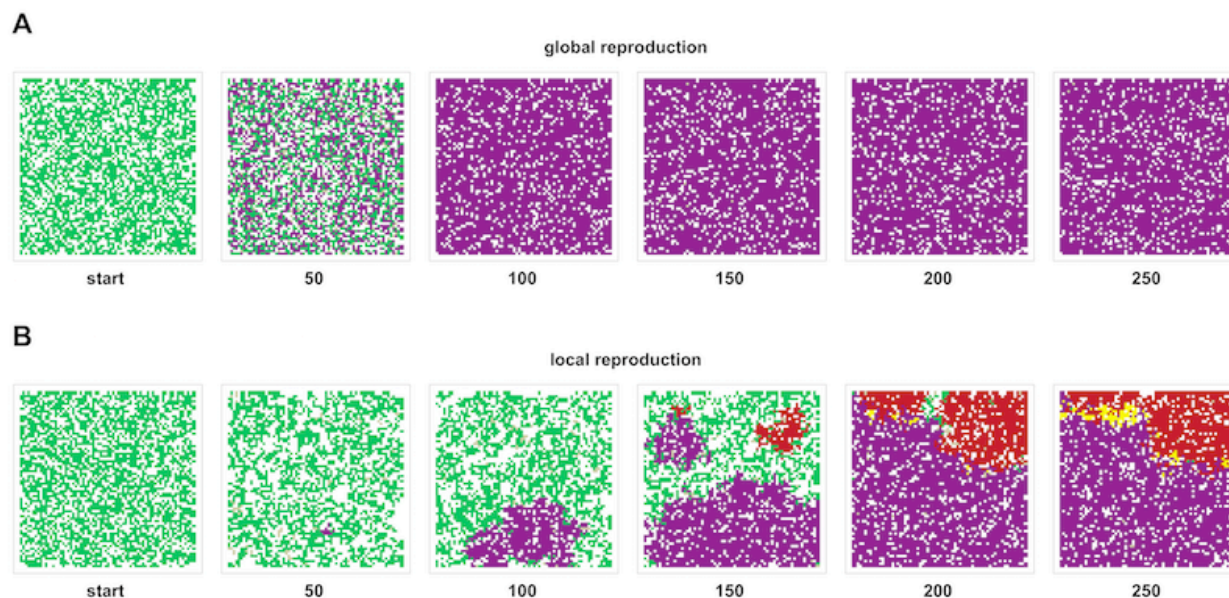
1077 On rugged fitness landscapes, populations may become trapped on a suboptimal fitness peak. It is also
1078 possible for a population to discover multiple distinct suboptimal peaks before any single peak
1079 genotype has fixed. Localized reproduction may promote the coexistence of multiple peaks by
1080 increasing the time-to-fixation of a newly discovered peak. Thus, localized reproduction may foster the
1081 diversity of genotypes required for peak-jumping via recombination (*e.g.*, the creation of peak
1082 genotype 1111 due to recombination between suboptimal peak genotypes 0011 and 1100). However,
1083 localized reproduction precludes peak-jumping unless the peak lineages are physically close. Physical
1084 proximity could result if two expanding peak lineages eventually abut, allowing meaningful
1085 recombination at the suture between the distinct genotypes. Such sutures between subpopulations may
1086 allow repeated discovery of genotypes in the domain of attraction of a higher fitness genotype. Indeed,
1087 in a representative simulation of intermediate recombination with local reproduction from Figure 1,
1088 multiple suboptimal peak genotypes coexist (0011 and 1100), and the globally optimal genotype
1089 (1111) is repeatedly created at the sutures between these subpopulations (Figure 2B, supplemental
1090 video). In a parallel representative run with global reproduction, no such sutures exist, because an
1091 intermediate genotype, once discovered, quickly sweeps to near fixation (Figure 2A, supplemental
1092 video).

1093

1094

1095

1096



1097

1098 **Figure 2.** Population snapshots of representative runs from Figure 1 with a recombination rate between
1099 adjacent loci of 0.1. When reproduction is global (A), a suboptimal peak (purple) fixes by epoch 100,
1100 rendering recombination ineffective. When reproduction is local (B), two suboptimal peaks (purple and
1101 red) exist by epoch 150, and these subpopulations expand to physical proximity by epoch 200. The
1102 optimal genotype (yellow) is then created multiple times via peak-jumping at the suture between the
1103 two suboptimal peaks.
1104

1105

1106 Does local reproduction encourage sutures between subpopulations? To test this, we simulate a two-
1107 locus landscape with two peak genotypes (10 and 01) and two valley genotypes (00 and 11, the latter
1108 of which is lethal). The population is initialized on genotype 00, and we track how frequently genotype
1109 11 is created, and how it is created. We find that genotype 11 is created by recombination more
1110 frequently in local rather than global reproductive schemes, while it is created by mutation at
1111 approximately the same frequency in the two schemes (Supplemental Figure 1).

1112

1113 **Local reproduction mitigates the loss of novel genotypes via recombination**

1114 Once a peak genotype is discovered, it may be lost due to subsequent recombination with unlike types,
1115 lowering the genotypic fidelity of its lineage. When recombination rates are high, such loss may
1116 prevent a genotype from establishing. However, spatially segregated populations may harbor
1117 population “centers”, in which mating pairs are likely to be genetically similar, preserving genotypic
1118 fidelity. Such centers may allow rare genotypes to persist in a population despite recombination. To
1119 examine the effect of centers on the establishment of a novel peak genotype, we model adaptation on a
1120 two-locus landscape in which a population may escape from suboptimal peak genotype 00 by crossing
1121 an adaptive valley (genotypes 10 and 01) to optimal peak genotype 11. We find a three-way interaction
1122 between recombination, reproductive distance, and centers ($p=0.03$, Manly’s permutation test).
1123 Frequent recombination slows the establishment of the optimal peak genotype in global but not local
1124 reproductive schemes (Figure 3, top row). However, if optimal peak genotypes are prohibited from
1125 mating with each other when rare (*i.e.*, when they comprise less than 1% of the population), the local
1126 and global reproductive schemes have similar results when recombination is frequent (Fig 3, bottom
1127 row).

1128

1129

1130

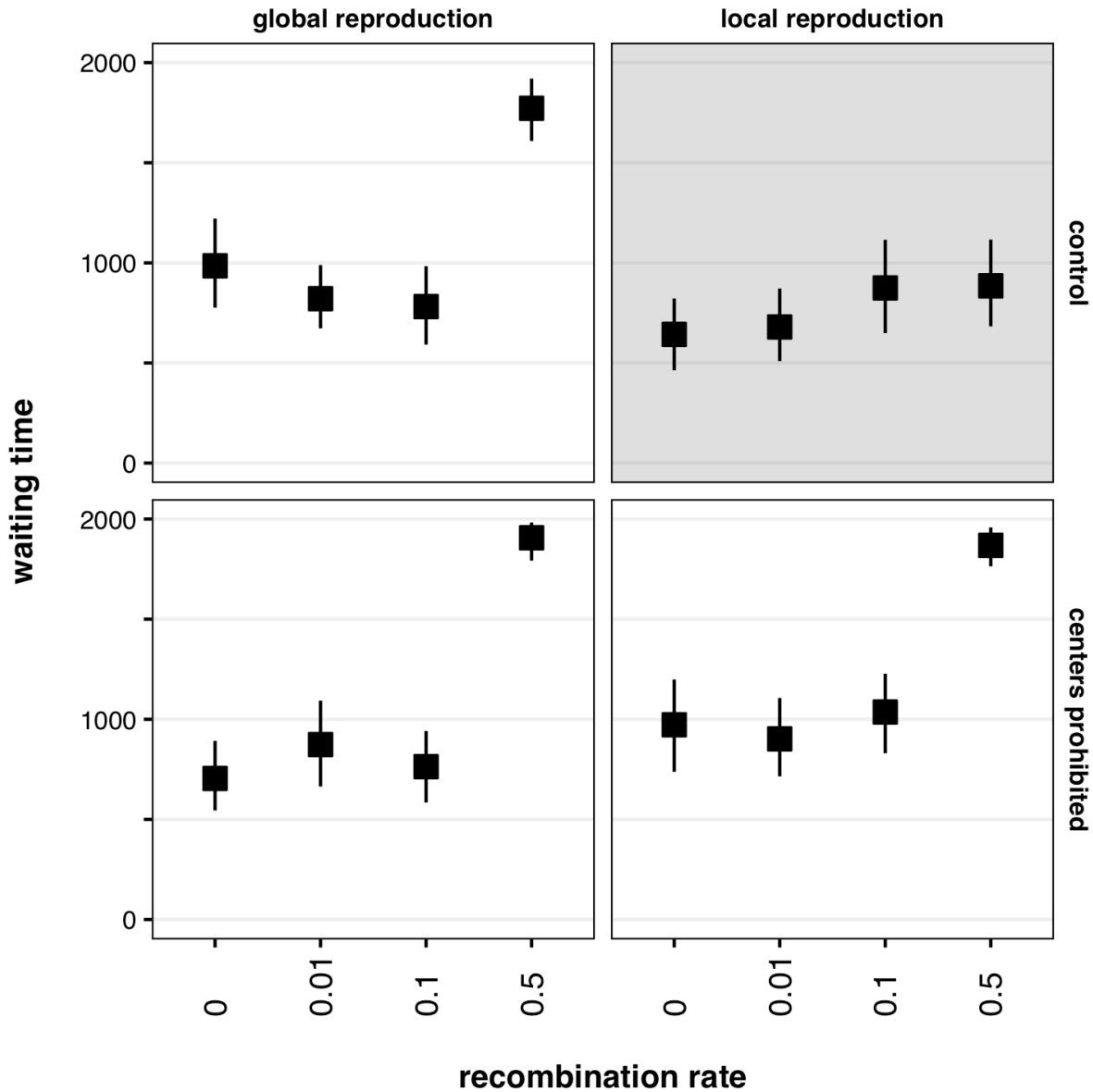
1131

1132

1133

1134

1135



1137

1138

1139

1140

1141

1142

1143

1144

1145

1146

1147

Figure 3. Waiting time to establishment of an optimal peak genotype at various recombination rates, with and without prohibiting “centers”. Populations are initialized on suboptimal peak genotype 00, and must cross an adaptive valley to optimal peak genotype 11. Clustered genotype centers allow nascent peaks to establish despite frequent recombination. When reproduction is global, frequent recombination prevents valley-crossing. Likewise, when genotype 11 individuals are prohibited from mating with each other until they have reached a frequency of 1% (“centers prohibited” treatments), frequent recombination prevents valley-crossing. However, local reproduction with naturally occurring clusters of rare genotypes (“centers”) allows valley-crossing even with frequent recombination (top-right, shaded). Data points and error bars represent mean values and standard error of 40 replicate simulations using parameter values $L = 70$, $\mu = 0.001$, $s_{00} = 0.8$, $s_{10} = s_{01} = 0.6$, $s_{11} = 0.9$.

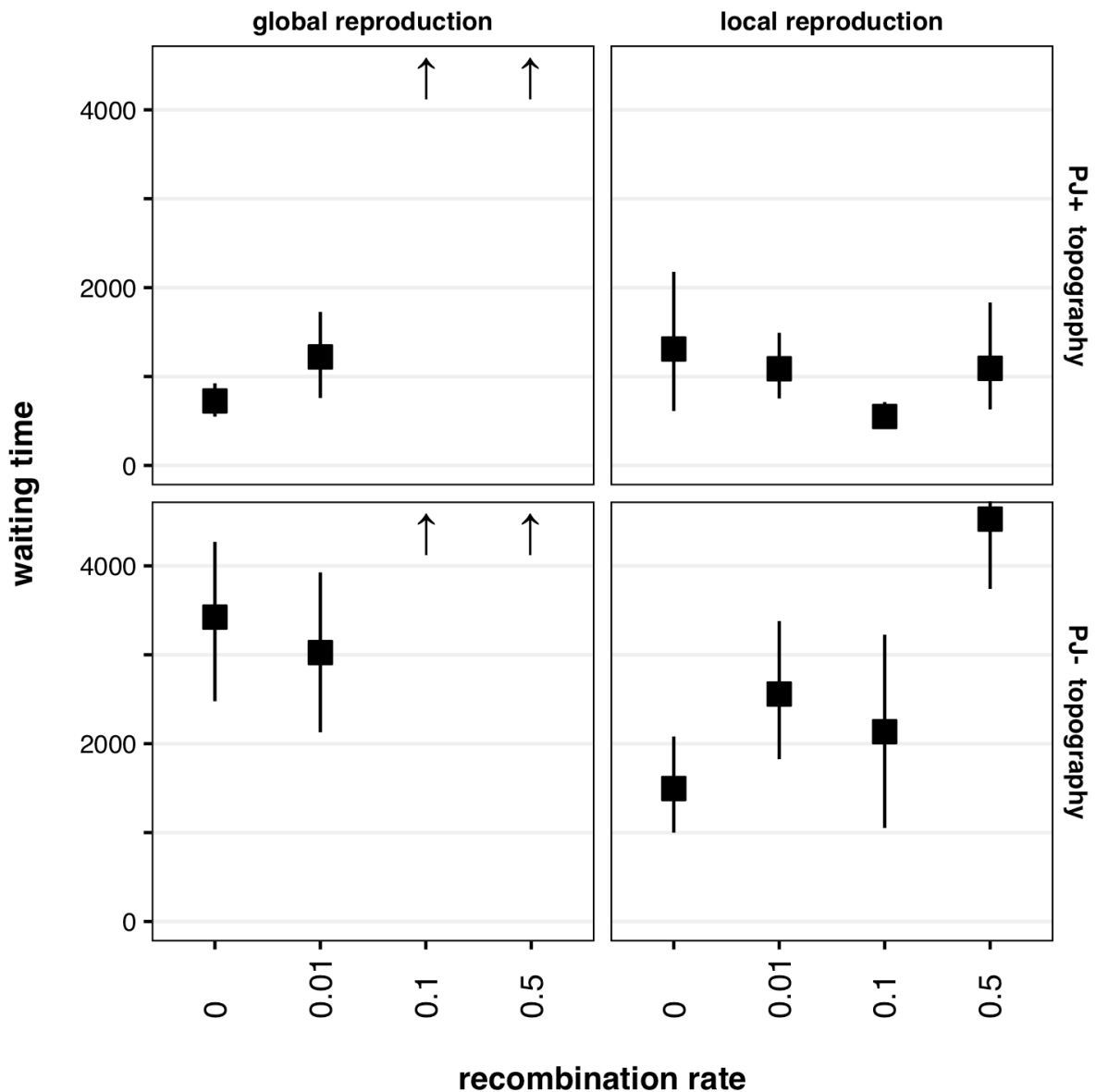
l148 While recombination may allow a population to more quickly climb a local peak, it can also trap
l149 populations on suboptimal peaks [17]. However, recombination may aid escape from suboptimal peaks
l150 if the landscape topography supports a diversity of genotypes and permits peak-jumping [14,19,24].
l151 Sutures should be most effective when recombination between two suboptimal peaks can create
l152 offspring in the attraction basin of a third, higher peak, allowing for peak-jumping. Centers should be
l153 most effective when novel peaks are discovered via peak-jumping, as recombination between the
l154 nascent peak and the majority genotypes can create low-fitness offspring. Thus the ability of sutures
l155 and centers to modulate the effects of recombination—to harness the creative aspect and mitigate the
l156 destructive aspect—may be sensitive to the particular topography of a rugged landscape.

l157

l158 **Sutures and centers in empirically derived fitness landscapes**

l159 The full topographies of some naturally occurring fitness landscapes have been measured for small
l160 subsets of their genotype spaces [25]. De Visser *et al.* [15] generated 5-locus empirical fitness
l161 landscapes by introducing deleterious mutations into the asexual fungus *A. niger*, and measuring the
l162 fitness effects of five individual mutations and all combinations thereof. Two complete 5-locus fitness
l163 landscapes were generated, with 32 genotypes each (though the landscapes are not completely
l164 independent as they share four of their five loci of interest). Both landscapes were found to be rugged,
l165 with multiple local maxima and minima. However, only one of the landscapes (which we call PJ⁺) had
l166 suboptimal peaks which could recombine into the attraction basin of the optimal peak; the other
l167 landscape (PJ⁻) did not. De Visser *et al.* found that recombination generally slows or halts the
l168 establishment of the optimal genotype in either landscape, though there was a window of very
l169 infrequent recombination that could speed adaptation in PJ⁺ and very slightly and rarely speed
l170 adaptation in PJ⁻ (see [15], supplement B1). We create landscapes parallel to PJ⁺ and PJ⁻ for our model

1171 (*e.g.*, replacing relative fitness with relative survival probabilities), and simulate evolution as before.
1172 We find a significant three-way interaction between recombination, reproductive distance, and fitness
1173 landscape topology on the waiting time for optimal genotype establishment ($p < 0.001$, Manly's
1174 permutation test). On PJ^+ , recombination slows or prevents the establishment of the optimal genotype
1175 when reproduction is global, but never slows or prevents adaptation when reproduction is local. On PJ^-
1176 , whose topography is less conducive to landscape exploration via recombination, we find similar
1177 results to PJ^+ when reproduction is global, but high recombination ($r=0.5$) still slows the generation
1178 and establishment of the optimal genotype when reproduction is local.



1179
 1180 **Figure 4.** Waiting time to establishment of optimal genotypes on empirically-derived rugged
 1181 landscapes at various recombination rates. When reproduction is global, recombination slows or
 1182 prevents the establishment of an optimal genotype (left column). Local reproduction mitigates the
 1183 slowing effect of recombination in both landscapes. In the landscape whose topography allows
 1184 recombination between suboptimal peaks to create an offspring in the attractive basin of the optimal
 1185 genotype—a landscape that permits peak-jumping—recombination can speed the establishment of the
 1186 optimal genotype (top-right panel). Data points and error bars represent mean values and standard error
 1187 of 15 replicate simulations using parameter values $L = 70$, $\mu = 0.001$. Upward arrows indicate that
 1188 establishment never occurred by the simulation maximum of 5000 epochs. For an explanation of the
 1189 conversion from relative fitnesses (as reported in [15] to comparable survival probabilities (as used in
 1190 this model), see Appendix.
 1191

l192 In our test landscape and in two empirically-derived landscapes, sufficiently high rates of
l193 recombination prohibit the establishment of a novel high-fitness peak when reproduction is global, but
l194 this destructive side of recombination is alleviated when reproduction is local. Moreover, in landscape
l195 topographies that allow peak-jumping (our test landscape and, to a lesser extent, PJ⁺), recombination
l196 can speed the establishment of novel high-fitness peaks. Thus, the landscape topography affects the
l197 ability of local reproduction to mediate the effects of recombination: accentuating exploration via
l198 “sutures” while mitigating recombinatory destruction of rare genotypes via “centers”. We suggest the
l199 greatest effect of sutures occurs when peak-jumping is possible, and the greatest effect of centers
l200 occurs when novel peaks are created via peak-jumping. Indeed, we see an amplified effect of local
l201 reproduction on a contrived fitness landscape with six suboptimal peaks and many opportunities for
l202 peak-jumping (Supplemental Figure 2). The prevalence of such topographical features and spatial
l203 restrictions—and therefore how relevant “sutures” and “centers” are to natural populations—remains
l204 an empirical question. It is possible, though, that by creating “sutures”, spatially structured populations
l205 may efficiently explore rugged landscapes via recombination, and by creating “centers”, those same
l206 populations may permit the establishment of novel peaks *despite* recombination. Spatially structured
l207 populations may therefore harness recombination’s constructive effects while mitigating its destructive
l208 effects on adaptation in rugged landscapes.

l209

l210

l211

l212

l213

l214

1215 **References**

- 1216 1. Otto SP, Lenormand T. Resolving the paradox of sex and recombination. *Nat Rev Genet.*
 1217 2002;3: 252–261. doi:10.1038/nrg761
- 1218 2. Otto SP, Gerstein AC. Why have sex? The population genetics of sex and recombination.
 1219 *Biochemical Society Transactions.* 2006;34: 519–522. doi:10.1042/BST0340519
- 1220 3. Fisher RA. *The Genetical Theory of Natural Selection: A Complete Variorum Edition.* OUP
 1221 Oxford; 1930.
- 1222 4. Muller HJ. Some Genetic Aspects of Sex. *The American Naturalist.* 1932;66: 118–138.
- 1223 5. Christiansen FB, Otto SP, Bergman A, Feldman MW. Waiting with and without recombination:
 1224 the time to production of a double mutant. *Theor Popul Biol.* 1998;53: 199–215.
 1225 doi:10.1006/tpbi.1997.1358
- 1226 6. Colegrave N. Sex releases the speed limit on evolution. *Nature.* 2002;420: 664–666.
- 1227 7. Cooper TF. Recombination Speeds Adaptation by Reducing Competition between Beneficial
 1228 Mutations in Populations of *Escherichia coli*. *PLOS Biol.* 2007;5: e225.
 1229 doi:10.1371/journal.pbio.0050225
- 1230 8. McDonald MJ, Rice DP, Desai MM. Sex speeds adaptation by altering the dynamics of
 1231 molecular evolution. *Nature.* 2016;531: 233–236. doi:10.1038/nature17143
- 1232 9. Poelwijk FJ, Tănase-Nicola S, Kiviet DJ, Tans SJ. Reciprocal sign epistasis is a necessary
 1233 condition for multi-peaked fitness landscapes. *Journal of Theoretical Biology.* 2011;272: 141–
 1234 144. doi:10.1016/j.jtbi.2010.12.015
- 1235 10. Altland A, Fischer A, Krug J, Szendro IG. Rare Events in Population Genetics: Stochastic
 1236 Tunneling in a Two-Locus Model with Recombination. *Phys Rev Lett.* 2011;106: 88101.
 1237 doi:10.1103/PhysRevLett.106.088101
- 1238 11. Jain K. Time to fixation in the presence of recombination. *Theoretical Population Biology.*
 1239 2010;77: 23–31. doi:10.1016/j.tpb.2009.10.005
- 1240 12. Weinreich DM, Chao L, Phillips P. Rapid evolutionary escape by large populations from local
 1241 fitness peaks is likely in nature. *Evolution.* 2005;59: 1175–1182. doi:10.1554/04-392
- 1242 13. Kondrashov FA, Kondrashov AS. Multidimensional epistasis and the disadvantage of sex.
 1243 *PNAS.* 2001;98: 12089–12092. doi:10.1073/pnas.211214298
- 1244 14. Watson RA, Weinreich DM, Wakeley J. Genome Structure and the Benefit of Sex. *Evolution.*
 1245 2011;65: 523–536. doi:10.1111/j.1558-5646.2010.01144.x
- 1246 15. de Visser JAGM, Park S-C, Krug J. Exploring the effect of sex on empirical fitness landscapes.
 1247 *Am Nat.* 2009;174 Suppl 1: S15-30. doi:10.1086/599081
- 1248 16. Moradigaravand D, Engelstädter J. The Effect of Bacterial Recombination on Adaptation on
 1249 Fitness Landscapes with Limited Peak Accessibility. *PLoS Comput Biol.* 2012;8: e1002735.
 1250 doi:10.1371/journal.pcbi.1002735
- 1251 17. Nowak S, Neidhart J, Szendro IG, Krug J. Multidimensional Epistasis and the Transitory
 1252 Advantage of Sex. *PLOS Comput Biol.* 2014;10: e1003836. doi:10.1371/journal.pcbi.1003836
- 1253 18. Moradigaravand D, Kouyos R, Hinkley T, Haddad M, Petropoulos CJ, Engelstädter J, et al.
 1254 Recombination Accelerates Adaptation on a Large-Scale Empirical Fitness Landscape in HIV-
 1255 1. *PLOS Genet.* 2014;10: e1004439. doi:10.1371/journal.pgen.1004439
- 1256 19. Crona K. Recombination and peak jumping. arXiv:14112017 [q-bio]. 2014; Available:
 1257 <http://arxiv.org/abs/1411.2017>

- 1258 20. Cooper JD, Neuhauser C, Dean AM, Kerr B. Tipping the mutation–selection balance: Limited
1259 migration increases the frequency of deleterious mutants. *Journal of Theoretical Biology*.
1260 2015;380: 123–133. doi:10.1016/j.jtbi.2015.05.003
- 1261 21. Martens EA, Hallatschek O. Interfering Waves of Adaptation Promote Spatial Mixing.
1262 *Genetics*. 2011;189: 1045–1060. doi:10.1534/genetics.111.130112
- 1263 22. Crow JF, Kimura M. *Evolution in Sexual and Asexual Populations*. *The American Naturalist*.
1264 1965;99: 439–450.
- 1265 23. Manly BFJ. *Randomization, Bootstrap and Monte Carlo Methods in Biology*, Third Edition.
1266 CRC Press; 2006.
- 1267 24. Watson RA, Jansen T. A Building-block Royal Road Where Crossover is Provably Essential.
1268 *Proceedings of the 9th Annual Conference on Genetic and Evolutionary Computation*. New
1269 York, NY, USA: ACM; 2007. pp. 1452–1459. doi:10.1145/1276958.1277224
- 1270 25. Szendro IG, Schenk MF, Franke J, Krug J, Visser JAGM de. Quantitative analyses of empirical
1271 fitness landscapes. *J Stat Mech*. 2013;2013: P01005. doi:10.1088/1742-5468/2013/01/P01005
1272

1273

1274

1275

1276

1277

1278

1279

1280

1281

1282

1283

1284

1285

1286

1287

1288 **Supplemental Figures**

1289

1290

1291

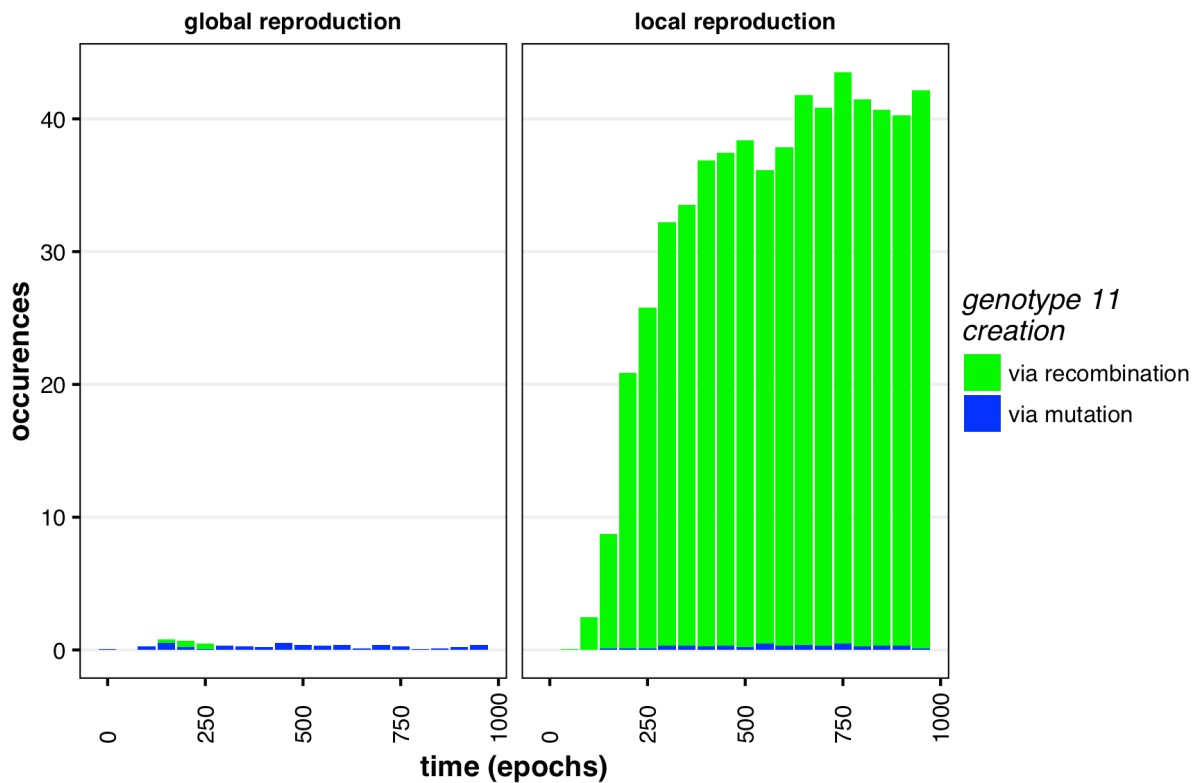
1292

1293

1294

1295

1296



1297

1298 **Supplemental Figure 1.** “Sutures” between suboptimal peaks allow landscape exploration.

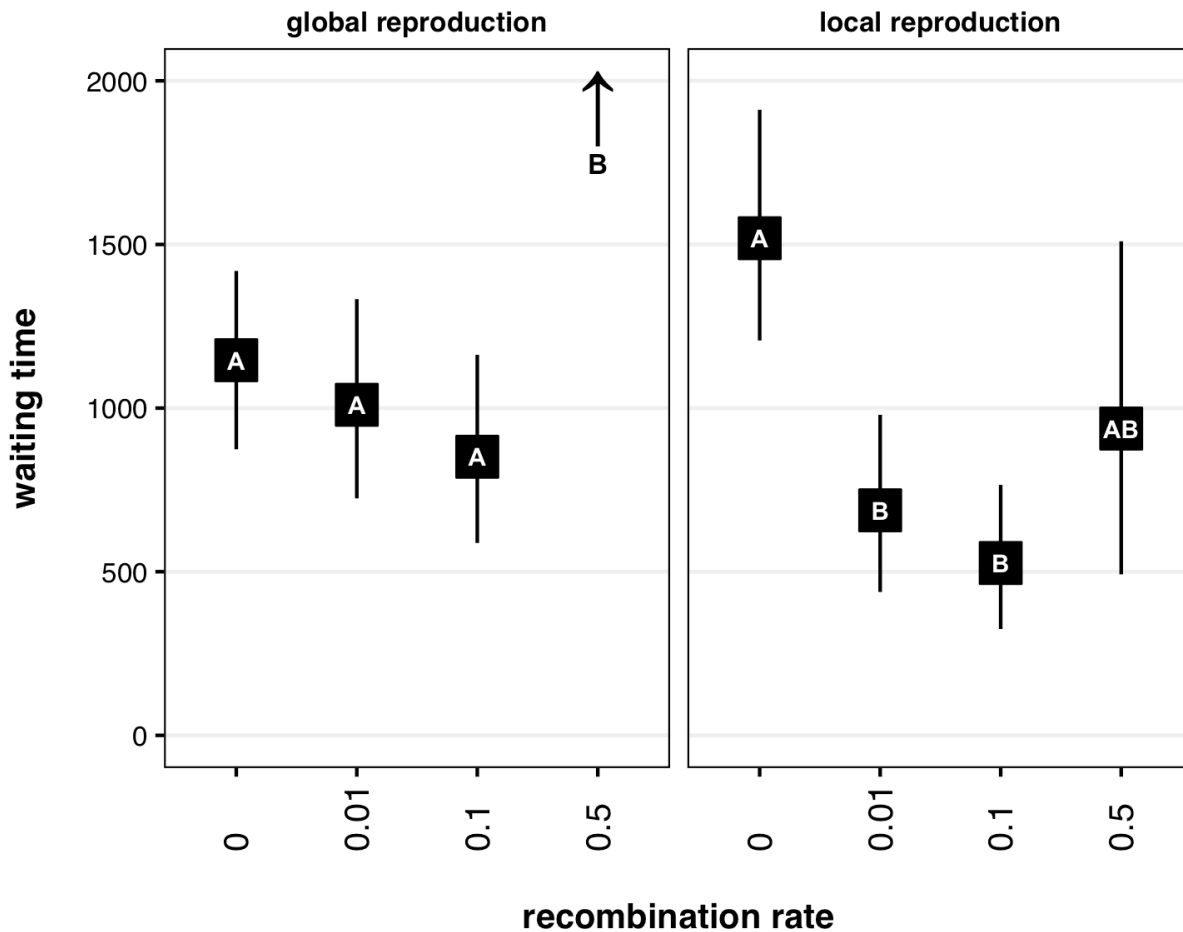
1299 Populations are initialized with genotype 00 on a fitness landscape with peak genotypes 01 and 10.

1300 Lethal genotype 11 is created via recombination (green bars) frequently only when reproduction is

1301 local. Genotype 11 is created via mutation (blue bars) at a low rate at both reproductive distances. Bars

1302 represent mean values of 15 replicate simulations using parameter values $L = 70$, $\mu = 10^{-5}$, $f_{11} = 0$,

1303 $s_{00} = 0.6$, $s_{10} = s_{01} = 0.85$, $s_{11} = 0$.



1304 **Supplemental Figure 2.** Similar to Figure 1, but with organisms of six loci (rather than four), and six
 1305 suboptimal peaks (rather than two). The pattern seen in Figure 1 appears more pronounced, likely due
 1306 to increased opportunity for peak-jumping. Data points and error bars represent mean values and
 1307 standard error of 25 replicate simulations using parameter values $L = 70$, $\mu = 0.002$, $s_G = 0.2$,
 1308 $s_{000000} = 0.6$, $s_{110000} = s_{001100} = s_{000011} = 0.85$, $s_{111100} = s_{110011} = s_{001111} = 0.9$, $s_{111111} =$
 1309 0.95 , where G represents all non-specified genotypes. Data points with no shared letter are
 1310 significantly different (Tukey's HSD, $\alpha = 0.05$). The upward arrow indicates that establishment never
 1311 occurred by the simulation maximum of 20,000 epochs.
 1312
 1313

1314

1315 [Supplemental Video]

1316 **Supplemental Video.** Population composition through time of the simulations depicted in Figure 2.
 1317 The starting genotype (0000) is represented by green; the two other suboptimal peak genotypes (0011
 1318 and 1100) are represented by red and purple, respectively; the optimal genotype (1111) is represented
 1319 by yellow. All other genotypes are represented by grey.
 1320

1321 **Appendix**

1322 De Visser et al (2009) created their empirical fitness landscapes (which they call CS1 and CS2) by
1323 measuring growth rates of all 32 relevant genotypes, and define relative fitness as a genotype's growth
1324 rate divided by the maximum growth rate of that landscape's genotypes. We convert these fitnesses
1325 (ω_G) to survival probabilities (s_G) with the formula $s_G = \frac{\omega_G}{2\bar{\omega}}$, where $\bar{\omega}$ is the average fitness on the
1326 landscape.

1327

1328

1329

1330

1331

1332

1333

1334

1335

1336

1337

1338

1339

1340

1341

1342

1343

genotype	PJ ⁺ (CS1)		PJ ⁻ (CS2)	
	ω_G	δ_G	ω_G	δ_G
00000	1.000	0.638	1.000	0.628
10000	0.878	0.560	0.878	0.551
01000	0.835	0.533	0.835	0.524
00100	0.870	0.555	0.870	0.546
00010	0.772	0.493	0.909	0.571
00001	0.793	0.506	0.772	0.485
11000	0.865	0.552	0.865	0.543
10100	0.854	0.545	0.854	0.536
10010	0.773	0.493	0.923	0.580
10001	0.873	0.557	0.773	0.485
01100	0.816	0.521	0.816	0.512
01010	0.716	0.457	0.852	0.535
01001	0.848	0.541	0.716	0.450
00110	0.778	0.497	0.855	0.537
00101	0.820	0.523	0.778	0.488
00011	0.972	0.620	0.785	0.493
11100	0.816	0.521	0.816	0.512
11010	0.748	0.477	0.879	0.552
11001	0.832	0.531	0.748	0.470
10110	0.749	0.478	0.942	0.592
10101	0.792	0.506	0.749	0.470
10011	0.753	0.481	0.795	0.499
01110	0.617	0.394	0.858	0.539
01101	0.810	0.517	0.617	0.387
01011	0.643	0.410	0.724	0.455
00111	0.671	0.428	0.745	0.468
11110	0.690	0.440	0.825	0.518
11101	0.855	0.546	0.690	0.433
11011	0.649	0.414	0.665	0.418
10111	0.692	0.442	0.686	0.431
01111	0.643	0.410	0.640	0.402
11111	0.645	0.412	0.622	0.391
mean	0.783	0.500	0.796	0.500
SD	0.095	0.061	0.095	0.060

l344

l345

l346

1347

1348

1349

1350

1351

1352

1353

1354

1355

1356

1357

1358

Chapter 3

1359

1360

1361

1362

1363

1364

1365

1366

1367

1368

1369

1370
1371
1372
1373
1374
1375
1376
1377
1378
1379
1380
1381
1382
1383
1384
1385
1386
1387
1388
1389
1390
1391
1392
1393
1394
1395
1396
1397
1398
1399
1400
1401
1402
1403
1404
1405
1406
1407
1408
1409
1410
1411
1412
1413
1414
1415

**David slays Goliath ‘discretely’:
Competitive reversals through oscillations and chaos**

Jacob D Cooper¹, Clarence Lehman², Richard McGehee³, and Benjamin Kerr¹

¹ *Department of Biology, University of Washington, Seattle, WA*

² *Department of Ecology, Evolution, and Behavior, University of Minnesota, Minneapolis, MN*

³ *School of Mathematics, University of Minnesota, Minneapolis, MN*

Running title:

David slays Goliath ‘discretely’

Corresponding author:

Benjamin Kerr
University of Washington
Department of Biology
Box 351800
Seattle, WA 98195-1800
phone: (206) 221-7026
email: kerrb@uw.edu

Keywords:

discrete population dynamics
Ricker model
coexistence
Hassell model
Lotka-Volterra

l416 **Abstract:**

l417 Many species reproduce in discrete bursts, often synchronized with the seasons. Although such
l418 discrete-time dynamics of single populations have been modeled systematically, the corresponding
l419 theory for multiple populations is less developed. Here we show that classical rules for predicting
l420 competitive outcomes are appropriate for a certain subset of discrete-time systems, which motivates a
l421 new discrete-time competitive exclusion principle. Nonetheless, classical rules can fail dramatically for
l422 other discrete-time systems. As a striking example, a classically inferior species (e.g., low K or high
l423 R^*) can drive a classically superior competitor (high K or low R^*) to extinction. The reasons relate to
l424 (1) the shifting of statistical moments in abundance accompanying population fluctuations (cycles or
l425 chaos), and (2) how such moments are filtered by non-linearities in the logarithm of growth curves. We
l426 discuss some implications of these results for competition theory as well as other applications,
l427 including management and epidemiology.

l428

l429

l430

l431

l432

l433

l434

l435

l436

l437

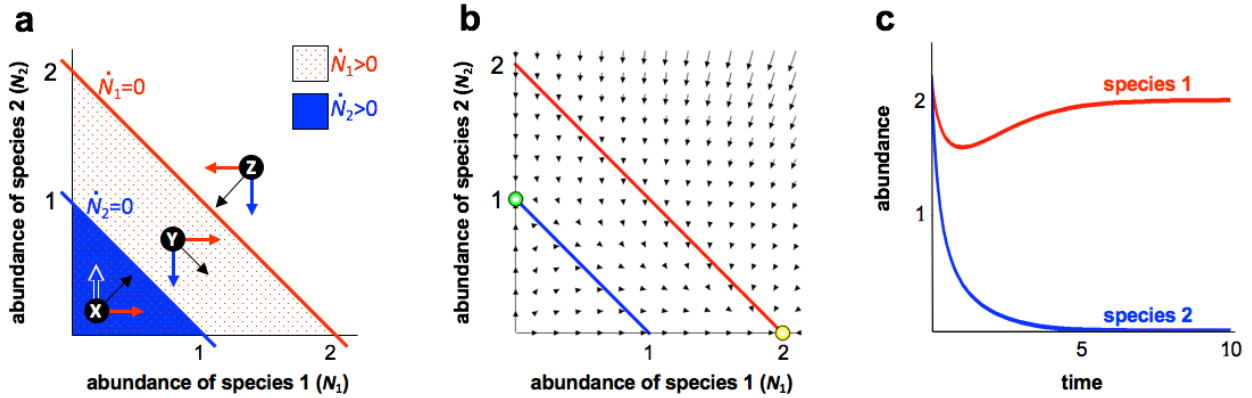
l438

1439 **Introduction**

1440 The introduction of discrete-time population dynamics into ecology was a theoretical bombshell
1441 (Hassell, 1975; Hassell and Comins, 1976; Hassell et al., 1976; May, 1974, 1975; May and Oster,
1442 1976). These early studies demonstrated that population dynamics resulting from structurally simple
1443 equations could be richly complex—exhibiting fixed points, cycles, and chaos. Indeed, erratic
1444 fluctuations in population data no longer required explanations of experimental error or stochastic
1445 noise, but rather could result from completely deterministic density-dependent population growth.
1446 There was also something of a heterodox character to these dynamics; discrete-time systems did not
1447 behave like their continuous-time counterparts. In this paper, we explore how discrete-time dynamics
1448 conform and deviate from expectations from continuous-time theory in the context of multiple
1449 competing species.

1450

1451 One of the simplest continuous-time models of ecological communities is the Lotka-Volterra
1452 framework for two-species competition. At any instant, the abundances of the two species are given by
1453 a point in a phase plane (Fig. 1). Movement of this point represents change in the competitors'
1454 abundances. The full dynamics can be discerned from the manner in which the zero-growth curves
1455 (isoclines) of the species are positioned. For example, in Figure 1a, the region in which species 1
1456 increases in abundance (dotted red region) completely encloses the corresponding region for species 2
1457 (solid blue region). There are no population values where species 1 decreases while species 2 increases
1458 (Figure 1b), and species 1 drives species 2 extinct (Figure 1c). This is a simple example of a more
1459 general exclusion principle proved by Volterra (1928) and explored empirically and philosophically by
1460 subsequent authors (*e.g.*, Gause, 1934; Hardin, 1960).



1462 **Figure 1:** Continuous-time competitor dynamics. (a) The dynamics of two competitors are given by
 1463 $dN_1/dt=(1-(N_1+N_2)/2)N_1$ and $dN_2/dt=(1-N_1-N_2)N_2$. The isoclines of species 1 and species 2
 1464 are red and blue, respectively. A point in the plane gives species' densities. For three example points (X, Y, and Z),
 1465 community change is given (roughly) by the black vector, which is broken into red (change in N_1) and
 1466 blue (change in N_2) components. The red-hatched and solid-blue regions indicate where N_1 and N_2
 1467 increase, respectively. (b) The corresponding slope field, showing locally stable (yellow circle) and
 1468 unstable (green circle) equilibria. (c) The community trajectory when $N_1(0)=N_2(0)=2.2$.
 1469

1470 Here we ask how such continuous-time theory translates to discrete-time. Does a species whose region
 1471 of increase completely encloses its competitor's (as in Fig. 1a) always have the competitive advantage?

1472 In fact, it is already known that two species can coexist under such circumstances (Adler, 1990;
 1473 Asmussen, 1979; Edmunds et al., 2003; Franke and Yakubu, 1991; Gatto, 1993). But, as we outline
 1474 below, a stranger turn of events is possible—a traditionally inferior species 2 can increase to high
 1475 abundance while driving species 1 extinct, even though at no instant of time does species 2 increase
 1476 while species 1 is decreasing. We turn to an example of such a scenario first.

1477

1478 **A Motivating Example**

1479 A generic discrete-time competition model for two species can be expressed as:

1480
$$N_1(t + 1) = G_1(N_1(t), N_2(t)) N_1(t) \tag{1a}$$

1481
$$N_2(t + 1) = G_2(N_1(t), N_2(t)) N_2(t) \tag{1b}$$

1482 where G_i is the factor by which the abundance of species i , N_i , increases ($G_i > 1$) or decreases ($G_i < 1$)
1483 from generation t to $t+1$. Since the species interact, G_i is a function of both species' abundances.
1484 Henceforth we assume that growth always slows with increasing abundances ($G_i \rightarrow 0$ as $N_1 \rightarrow \infty$ or
1485 $N_2 \rightarrow \infty$) and both species thrive when abundances are low ($G_i > 1$ when $N_1 \approx 0$ and $N_2 \approx 0$).

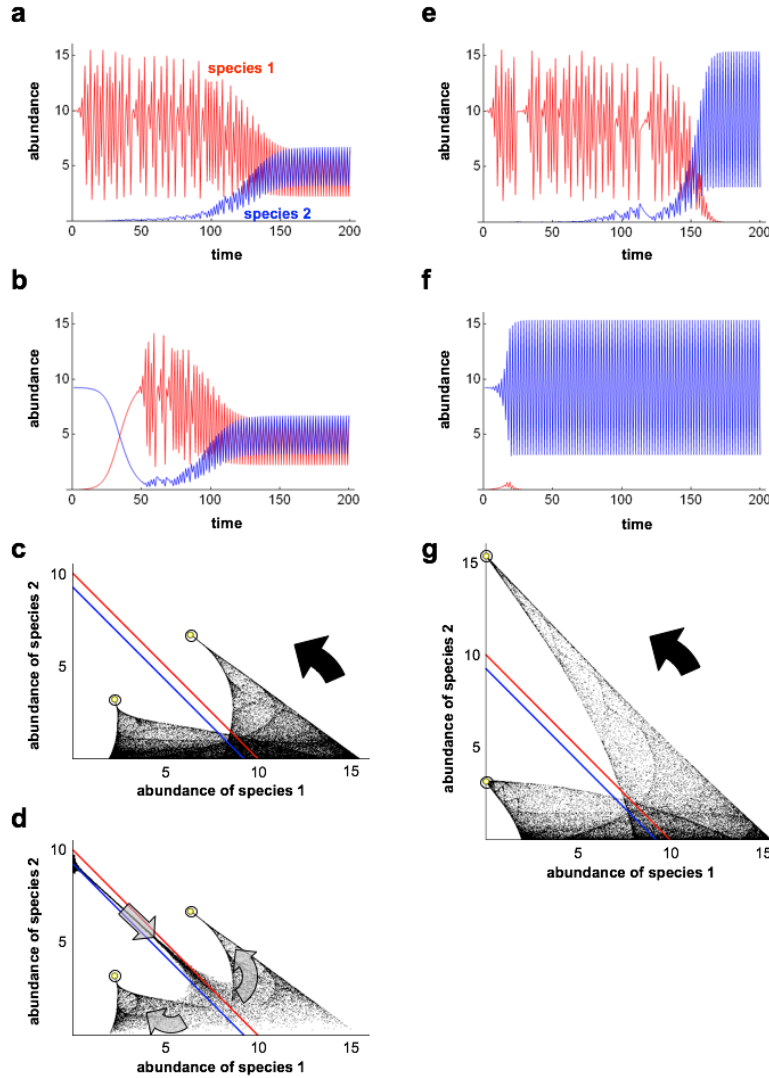
1486

1487 As a concrete example, consider an extended version of the widely-used Ricker model (Gatto, 1993;
1488 May, 1974; Ricker, 1954). In this model,

1489
$$G_i(N_1(t), N_2(t)) = \exp\{\ln(r_i)(1 - [(N_1(t) + N_2(t))/K_i]^{\gamma_i})\}$$

1490 where r_i is the growth factor when abundances are low, K_i is the carrying capacity, and γ_i is a 'shape
1491 parameter' for species i . This model is a discrete-time incarnation of the theta-logistic (Nelder, 1961).

1492 In Figure 2, the region of positive growth for species 1 completely encloses that of species 2. We might
1493 expect species 1 to out-compete species 2, which is what the isocline arrangement would dictate if
1494 reproduction were continuous (*e.g.*, Fig. 1). In fact, species 2 invades from low abundance and coexists
1495 with species 1 (Figs. 2a,c). Species 1 likewise invades and coexists (Figs. 2b,d). At higher growth rates
1496 of species 2, though the isoclines are unchanged, species 2 invades and displaces species 1 (Figs. 2e,g).
1497 The classically superior species 1 cannot invade species 2 (Fig. 2f). It seems we have a competitive
1498 David slaying Goliath. What is going on?



1499
 1500 **Figure 2:** Discrete-time competitor dynamics. (a) Dynamics of two competitors with
 1501 $G_i = \exp\{\ln(r_i)(1 - [(N_1(t) + N_2(t))/K_i]^{\gamma_i})\}$, where $r_1=4.4$, $r_2=6$, $K_1=10$, $K_2=9.25$, $\gamma_1=2$, and $\gamma_2=1$. The isoclines
 1502 do not cross and species 1 is the classically superior competitor. Nonetheless, species 2 invades and
 1503 coexists with species 1. (b) Coexistence also results when species 1 starts rare and species 2 begins near
 1504 its fixed point. (c) A phase plane representation of the dynamics from part a. We ran 500 simulations
 1505 with different initial conditions where a small point giving abundances was plotted for 1000 time steps
 1506 each. The community starts near species 1's axis and proceeds (curved black arrow) through oscillations
 1507 of decreasing complexity to a period-2 cycle with both species coexisting (yellow circles with rings).
 1508 The isoclines are also shown. (d) A phase plane representation of the dynamics from part b (500
 1509 simulations). The community moves off species 2's axis toward extinction of species 1 (straight grey
 1510 arrow) until oscillations develop and the community turns around (curved grey arrows), approaching
 1511 the same period-2 cycle. (e) The model from part a, except with $r_2=11$. Species 2 now *replaces* species 1
 1512 when starting from a low abundance. (f) Species 2 resists invasion by species 1. (g) A phase plane
 1513 representation (500 simulations) of the dynamics from part e. The chaotic trajectory on the N_1 axis is
 1514 unstable to invasion by species 2 (curved black arrow), whereas the period-2 cycle on the N_2 axis is
 1515 stable to invasion by species 1 (yellow circles with rings).

1516 Oscillations are a conspicuous feature in Figure 2. Coexistence of multiple species on fewer resources
 1517 than predicted by classical theory has been shown to occur when populations oscillate periodically or
 1518 chaotically, in both continuous-time (Armstrong and McGehee, 1980; Huisman and Weissing, 1999;
 1519 Vandermeer et al., 2002) and discrete-time (Adler, 1990; Asmussen, 1979; Edmunds et al., 2003;
 1520 Franke and Yakubu, 1991; Gatto, 1993). When systems are oscillating, conclusions based on equilibria
 1521 (or isoclines) can be unreliable. Is it ever reasonable to expect information about where abundance is
 1522 static (*e.g.*, equilibria) to say something useful about systems where abundance is perpetually
 1523 changing? Interestingly, the answer is ‘yes.’ For a class of common discrete-time systems, equilibria
 1524 tell the *whole* story about competitive outcomes, even when the system oscillates wildly and never
 1525 reaches equilibrium. For such systems we present and prove a competitive exclusion principle, which
 1526 corresponds to expectations from continuous-time theory (Volterra, 1928). We then show how models
 1527 outside of this class (*e.g.*, Fig. 2) can overturn our expectations.

1528

1529

1530 **Discrete-Time Competitive Exclusion Principle**

1531 Consider a community of S competitors in which the dynamics of species i is:

$$1532 \quad N_i(t + 1) = G_i(\mathbf{N}(t))N_i(t) \quad (2)$$

1533 where $\mathbf{N}(t) \equiv \langle N_1(t), N_2(t), N_3(t), \dots, N_S(t) \rangle$ gives the abundances of each species at t . Equation (2)

1534 generalizes equation (1). Let $\mathbf{N}_i(t) \equiv \langle 0, 0, 0, \dots, 0, N_i(t), 0, \dots, 0 \rangle$, where only species i is present (at

1535 density $\mathbf{N}_i(t)$); and $\vec{\mathbf{0}} \equiv \langle 0, 0, 0, \dots, 0 \rangle$, where all species are absent.

1536

1537 Here we describe competition for a type of common “abiotic resource” (*sensu* Armstrong and

1538 McGehee, 1980). We will call a community “Volterrian” if the logarithm of each growth factor can be

1539 written as follows:

1540
$$\ln G_i(\mathbf{N}(t)) = \alpha_i - \beta_i H(\mathbf{N}(t)) \tag{3}$$

1541 where $i \in \{1, 2, 3, \dots, S\}$, and with $\alpha_i > 0$ and $\beta_i > 0$. H is a continuous function with $H(\mathbf{0}) = 0$,

1542 $\partial H / \partial N_i > 0$, and $\lim_{N_j \rightarrow \infty} H(\mathbf{N}) = \infty$, for all $j \in \{1, 2, 3, \dots, S\}$ and any \mathbf{N} . Finally, we require that

1543 $H(\mathbf{N}_i) = H(\mathbf{N}_j)$ whenever $\|\mathbf{N}_i\| = \|\mathbf{N}_j\|$ (we note that the norm $\|\mathbf{N}_i(t)\| = N_i(t)$ here). The function H

1544 gauges the negative impact of species on the shared “abiotic resource.” Condition (3) describes a class

1545 of models that includes familiar members (Table 1).

1546

1547

Table 1: Models obeying the competitive exclusion principle

Model*	Growth Factor (G_i)	Single-Species Equilibrium (\bar{N}_i)	Condition (3) Details†		
			α_i	β_i	$H(x)$
Ricker‡	$\exp \left\{ \ln r_i \left[1 - \left(\frac{\sum_{j=1}^S N_j(t)}{K_i} \right)^\gamma \right] \right\}$	K_i	$\ln r_i$	$\frac{\ln r_i}{K_i}$	x^γ
Hassell§	$\frac{\lambda_i}{(1 + a \sum_{j=1}^S N_j(t))^{b_i}}$	$\frac{\exp(\lambda_i/b_i) - 1}{a}$	$\ln \lambda_i$	b_i	$\ln(1 + ax)$
Unnamed	$\lambda_i \left\{ \exp \left(1 - \exp \left(\sum_{j=1}^S N_j(t) \right) \right) \right\}^{w_i}$	$\ln(\ln v_i/w_i + 1)$	$\ln v_i$	w_i	$\frac{\exp(x) - 1}{-1}$

1548

1549 † In all cases shown the variable x is total abundance: $x = \sum_{j=1}^S N_j(t)$

1550 * In all of the models presented, standard competition coefficients are assumed to be unity

1551 ‡ This is an extended version of the standard Ricker model (as normally $\gamma=1$).

1552 § In this version of the Hassell model, the parameter a is assumed to be the same for every competitor.

1553

1554 In a Volterrian community, if species k has the highest equilibrium abundance when alone, it will

1555 displace all other species. We prove this in Appendix A and show how a community can be isolated to

1556 a shifting lower-dimensional subspace during its trajectory. Thus, condition (3) yields a competitive

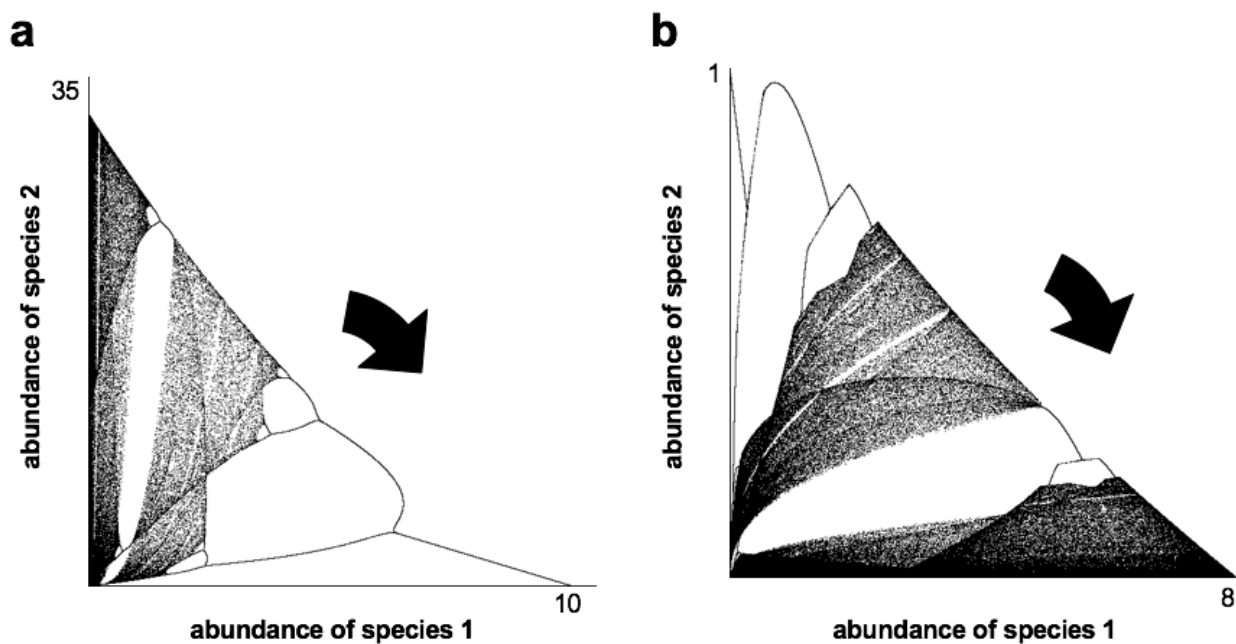
1557 exclusion principle, which operates regardless of oscillations (Supplementary Information, section
1558 B.7). Even if trajectories are chaotic, in Volterrian communities, there is order in the chaos.

1559

1560 In Figure 3, the equilibrium abundance of species 1 is slightly greater than species 2 for two
1561 communities satisfying condition (3). Despite oscillations, species 1 displaces species 2, dynamically
1562 etching a bifurcation diagram in the phase plane. This outcome is in agreement with the classical
1563 expectations based on isocline or other analyses.

1564

1565



1566

1567 **Figure 3:** Illustrations of the competitive exclusion principle. (a) The Ricker model (Table 1) with $r_1=3$,
1568 $r_2=30$, $K_1=10$, $K_2=9.995$, $\gamma=1$. A phase plane representation in which species 1 starts out rare and species
1569 2 starts out common. We ran 10 simulations (80,000 time steps each) with slightly different initial
1570 conditions, plotting a small point for abundances at each time step. The community starts near species
1571 2's axis and proceeds (curved black arrow) through oscillations of decreasing complexity to a fixed point
1572 with species 1 excluding species 2. (b) The Hassell model (Table 1) with $\lambda_1=150$, $\lambda_2=8$, $b_1=7.2284$, $b_2=3$,
1573 $a=1$. The community starts near species 2's axis and proceeds (curved black arrow) through oscillations
1574 of increasing complexity to a chaotic trajectory with species 1 excluding species 2.

1575

1576 **Explaining Unexpected Outcomes**

1577 Communities that do not satisfy condition (3) can violate classical expectations. Consider a two-
1578 species community where species 1 is a resident and species 2 is a rare invader. When extremely rare,
1579 the appropriate measure for the invader's long-term growth is $\widetilde{G}_2 = \lim_{T \rightarrow \infty} \sqrt[T]{\prod_{t=0}^{T-1} G_2(N_1(t), 0)}$.
1580 Mathematically, \widetilde{G}_2 is a Lyapunov number (Ferriere and Gatto, 1995; Gatto, 1993; Hastings et al.,
1581 1993; Metz et al., 1992). For species 2 to increase from rarity, \widetilde{G}_2 must exceed 1. Using an approach
1582 similar to Chesson's (2000), this growth rate can be approximated as:

1583
$$\widetilde{G}_2 \approx G_2(\overline{N}_1, 0) e^{(\delta_2/2)\sigma_{N_1}^2}, \quad (4a)$$

1584 where

1585
$$\delta_2 = \left. \frac{d^2 \ln G_2(n, 0)}{dn^2} \right|_{n=\overline{N}_1} \quad (4b)$$

1586 Equations (4) define an 'invasion heuristic' (Appendix B outlines the derivation for two species and
1587 the heuristic is generalized in the Supplementary Information, section C). Because our invasion
1588 heuristic highlights measurable quantities, such as the mean (\overline{N}_1) and variance ($\sigma_{N_1}^2$) in resident
1589 abundance, it is an empirically useful approximation of the Lyapunov number (see Ferriere & Gatto
1590 (1995) for details on Lyapunov analysis). The heuristic is generally suitable when the fluctuations in
1591 the resident's abundance are small.

1592

1593 A smaller mean abundance in a fluctuating resident, \overline{N}_1 , will make $G_2(\overline{N}_1, 0)$ greater, which helps the
1594 invader. The effect of the variance in resident abundance, $\sigma_{N_1}^2$, depends on the sign of δ_2 , which reflects
1595 the curvature of the invader's growth function. If $\ln G_2$ is concave ($\delta_2 < 0$), then a lower variance in the
1596 resident's abundance will make $e^{(\delta_2/2)\sigma_{N_1}^2}$ larger, helping the rare species invade. On the other hand, if
1597 $\ln G_2$ is convex ($\delta_2 > 0$), a higher resident variance helps the rare species.

1598 Thus, in the first approximation, successful invasion depends on the shape of the invader's growth
1599 function and on the statistical moments of the resident's population distribution. Such moments change
1600 with parameter values like the resident's intrinsic growth rate, r_1 . The bifurcation diagrams in Figure 4
1601 show how the variance of the resident tends to increase with r_1 . If the resident oscillates, its mean
1602 abundance is affected by the shape of its own growth curve. If the logarithm of the resident's growth
1603 function is concave, then the mean abundance of a fluctuating population is less than its single-species
1604 equilibrium. However, if the fluctuating resident's growth function is log-convex, then mean
1605 abundance is greater than its single-species equilibrium (Supplementary Information, section A.4). In
1606 general, if the resident's growth function is log-concave, larger oscillations will lower average
1607 abundance; whereas if the growth function is log-convex, oscillations will raise average abundance
1608 (Figs. 4a and 4c).

1609

1610

1611

1613 **Figure 4:** Effects of growth function log-concavity. (a) For a single-species Ricker model (Table 1), if
1614 $\gamma > 1$, $\ln G$ is concave (inlet: $\gamma = 2$). The bifurcation diagram gives long-term abundances as a function of
1615 intrinsic growth rate (more intensely visited regions are darker grey). The mean abundance (red line)
1616 decreases below the carrying capacity as fluctuations develop. (b) When $\gamma = 1$, $\ln G$ is linear. The mean
1617 abundance does not deviate from the carrying capacity as fluctuations develop. (c) When $\gamma < 1$, $\ln G$
1618 is convex (inlet: $\gamma = 1/2$). As fluctuations develop, the mean abundance increases above the carrying
1619 capacity. (d) A two-species model with $G_i = \exp\{\ln(r_i)(1 - [(N_1(t) + N_2(t))/K_i]^\gamma)\}$ and $r_{\text{inv}} = 11$, $K_{\text{res}} = 10$,
1620 $K_{\text{inv}} = 9.25$. We use $\gamma_i = 2$, $\gamma_i = 1$, and $\gamma_i = 0.5$ for log-concave, log-linear, and log-convex growth,
1621 respectively. From classical analysis, the resident is “superior.” We plot the invader’s long-term growth
1622 ($\widetilde{G}_{\text{inv}}$) in terms of the resident’s intrinsic growth rate (r_{res}) for different log-concavity combinations. The
1623 dots are from (4), using simulated resident moments. The jagged line is the invader’s growth computed
1624 as the long-term geometric mean. For $\gamma_{\text{inv}} = 1$ or $\gamma_{\text{inv}} = 2$, approximation (4) is exact. When $\gamma_{\text{inv}} = \gamma_{\text{res}}$ our
1625 exclusion principle applies (row 1, Table 1). However, when the “inferior” invader has a growth function
1626 that is more log-convex than the “superior” resident, then the invader’s long-term growth factor can be
1627 greater than unity (i.e., it can invade). This can be due to a “mean effect”: the oscillation-mediated
1628 reduction in the resident’s mean abundance (2nd row, 1st column); a “variance effect”: the oscillation-
1629 mediated increase in the invader’s effective growth (3rd row, 2nd column); or both (3rd row, 1st column).
1630 (e) The same model as in part d, except $r_{\text{inv}} = 4.4$, $K_{\text{res}} = 9.25$, $K_{\text{inv}} = 10$. Now the invader is “superior.”
1631 Approximation (4) can be inaccurate, as seen when both species have log-convex growth. The “superior”
1632 competitor may not be able to invade (long-term growth drops below unity) due to a “mean effect”, a
1633 “variance effect” or both (plots above the diagonal). Figure 2 can be understood by making species 1 the
1634 “superior” and species 2 the “inferior” and looking at the plot in 2nd row and 1st column of part d and the
1635 plot in the 1st row and 2nd column of part e.
1636

1637

1638 Now it can be seen why a traditionally inferior competitor need not be inferior under discrete
1639 reproduction. When species 1 in Figure 2 is alone with a low growth rate (r_1), its abundance is equal to
1640 its carrying capacity (K_1). However, at higher growth rates, species 1 can oscillate. For the parameters
1641 in Figures 2a-d, species 1 follows a chaotic trajectory if alone. Because the growth function of species
1642 1 is log-concave, oscillations lower its mean abundance below K_1 . Consequently, as an invader, species
1643 2 ‘feels’ a lower abundance of its competitor, on average, than it would if species 1 were at its fixed
1644 point. Given that the growth curve of species 2 is log-linear, the invading species 2 is aided by species
1645 1’s changed mean (lower $\overline{N_1}$ increases \widetilde{G}_2) while it is unaffected by species 1’s changed variance
1646 (higher $\sigma_{N_1}^2$ does not change \widetilde{G}_2 when $\delta_2 = 0$).

1647 The same analysis is relevant when considering species 2 as the resident and species 1 as the invader
1648 (i.e., $\widetilde{G}_1 \approx G_1(0, \overline{N}_2) e^{(\delta_1/2)\sigma_{N_2}^2}$ with $\delta_2 = \{d^2 \ln G_2(n, 0)/dn^2\}|_{n=\overline{N}_1}$). Consider the case of
1649 coexistence (Figs. 2a-d). Here, species 2 approaches its carrying capacity when alone (r_2 small—see
1650 Fig. 4b). In such a case, $\sigma_{N_2}^2 = 0$, $\overline{N}_2 = K_2$, and $G_1(0, K_2) > 1$. Consequently, $\widetilde{G}_1 > 1$ and species 1
1651 can invade. Thus, for Figures 2a-d, $\widetilde{G}_1 > 1$ and $\widetilde{G}_2 > 1$. In this case, coexistence results.

1652

1653 However, what happens if the intrinsic growth of species 2 increases, such that it oscillates when
1654 alone? In such a case, $\sigma_{N_2}^2 > 0$ and $\overline{N}_2 = K_2$ (due to log-linear growth). Given that species 1's growth
1655 is log-concave, the variance in species 2 harms the invasion potential of species 1 (\widetilde{G}_1 decreases as $\sigma_{N_2}^2$
1656 increases when $\delta_1 < 0$). It is possible for $\widetilde{G}_1 < 1$ if the variance in species 2 is large enough. The end
1657 result is that species 2 replaces species 1 (Figs. 2e-g)—opposite of expectations from continuous-time
1658 theory and our exclusion principle (compare the axis bearing yellow circles in Fig. 2g to that in Fig.
1659 1b). Such reversals can also occur in the simplest resource-based competition models. R^* is a
1660 measurable resource level below which a given species grown in monoculture cannot persist (Tilman,
1661 1982). Classically, the species with the lowest R^* displaces its competitors. Yet when reproduction
1662 occurs discretely, a species with a higher R^* can displace one with a lower R^* (Supplementary
1663 Information, section D.3).

1664

1665 In the case of Figure 2, condition (3) is violated because $\gamma_1 \neq \gamma_2$. When $\gamma_1 = \gamma_2 = \gamma$, condition (3) is satisfied
1666 (Table 1) and classical expectations hold (Fig. 3a). The parameter γ_i controls the log-concavity of the
1667 growth function of species i . By setting $\gamma_1 = 2$ and $\gamma_2 = 1$, the log-concavities of the two species differ (a
1668 form of relative non-linearity (Chesson, 2000)). As a resident, species 1 is harmed by its own
1669 fluctuations. As an invader, species 1 is harmed by the fluctuations in species 2. Meanwhile, species 2

1670 is not directly affected by fluctuations in the system. Thus, as the community experiences larger
1671 fluctuations (as r_1 and r_2 increase), the outlook for species 2 can improve to the point of exclusion of
1672 the classically superior species 1. Given differences in log-concavity, changes to the mean resident
1673 abundance (\bar{N}_i), variance in resident abundance ($\sigma_{N_i}^2$), or both simultaneously can lead to a reversal of
1674 fortune for an invader (Figs. 4d,e). Growth log-concavities are critical because the shape of the growth
1675 curve affects the mean abundance of a resident as well as the way that an invader ‘filters’ the variance
1676 in a resident.

1677

1678 **Discussion**

1679 The ecological theory of interacting species has developed over almost a century and has illuminated a
1680 diversity of applications, including management of wildlife populations, harvesting of natural
1681 resources, and control of epidemics. Much of this theory concerns species that reproduce continuously
1682 throughout the year, yet many species in nature reproduce only at discrete times, often synchronised
1683 with the seasons.

1684

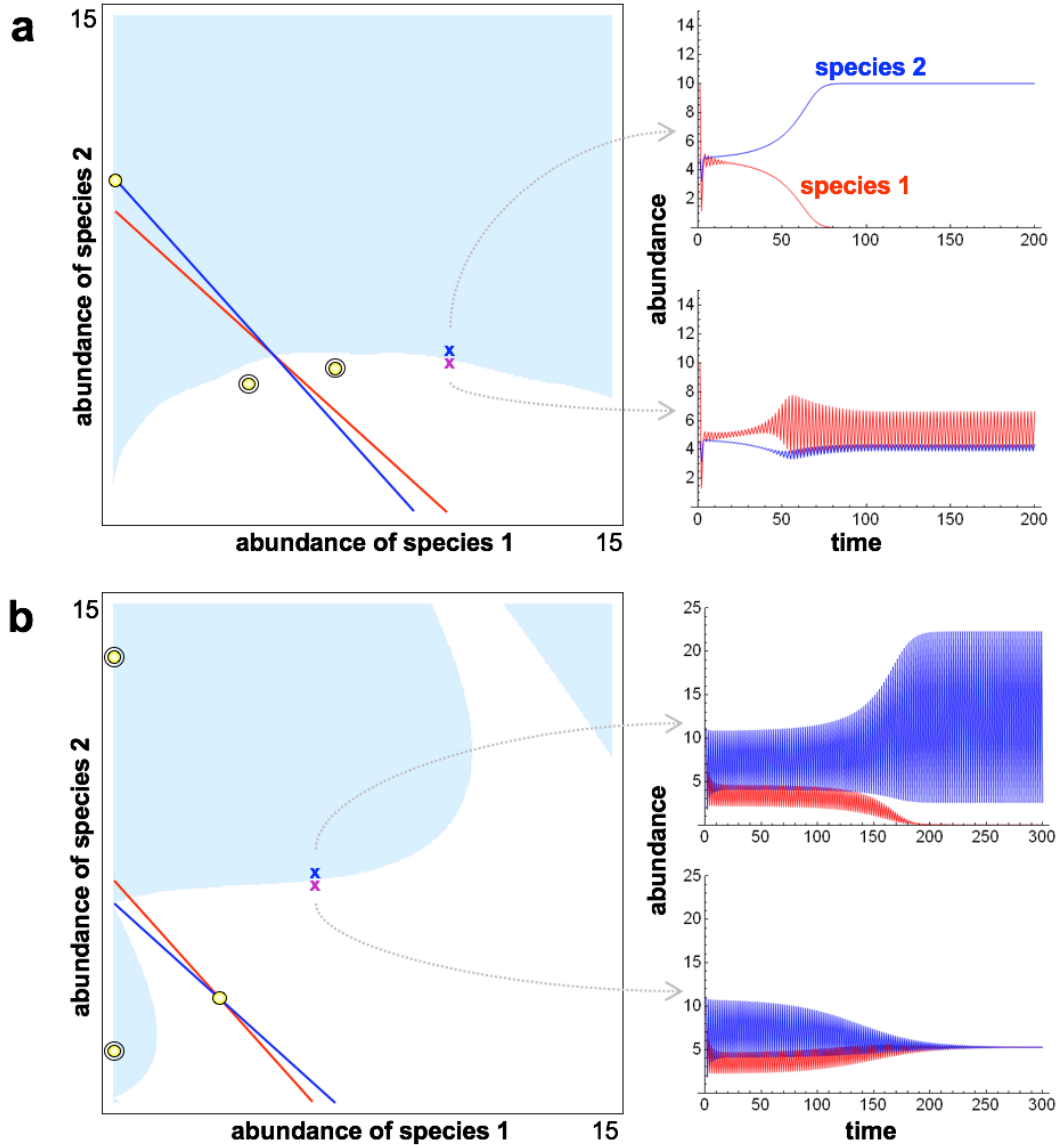
1685 In May’s classic paper, he outlined how simple density dependent growth in a single species in a
1686 discrete-time framework could produce dynamics foreign to an equivalent continuous-time framework
1687 (May, 1974). At the end of the very same paper, May discussed deviation between a discrete-time two-
1688 species version of the Lotka-Volterra model and its continuous-time equivalent. The continuous-time
1689 Lotka-Volterra model predicts four basic competitive outcomes depending on the orientation of
1690 isoclines: (i) species 1 excludes species 2, (ii) species 2 excludes species 1, (iii) both species coexist, or
1691 (iv) either species can exclude the other depending on initial conditions (bistability). For discrete
1692 models that do not satisfy condition (3), we have shown that expectations based on this Lotka-Volterra
1693 framework can be misleading. Indeed, all four dynamical outcomes are consistent with a single

1694 isocline arrangement (Supplementary Information, section D.1). Furthermore, novel outcomes are
1695 possible and lead to potential applications in the laboratory and the field.

1696

1697 A first sample application is Park's famous *Tribolium* competition experiments. These have often been
1698 interpreted using the standard Lotka-Volterra taxonomy (see Edmunds *et al.* (2003) for a historical
1699 overview), in spite of the fact that Park discovered unconventional competitive outcomes in a final
1700 experiment with two competitors (Leslie *et al.*, 1968). In most of the competitions, Park observed that
1701 one species excluded the other (consistent with bistability); but, in one competition, the two species
1702 were found to coexist over 30 generations. Discrete time models incorporating life cycle stages (e.g.,
1703 larvae, pupae, and adults) have showcased the existence of multiple attractors corresponding to both
1704 coexistence and exclusion that are consistent with these results (Cushing *et al.*, 2004; Edmunds *et al.*,
1705 2003). However, it has been posed as an open question (Cushing *et al.*, 2004) whether simple
1706 competition models without explicit life cycle stages (such as the two-species Ricker) can also
1707 demonstrate such dynamics. Figures 5a and 5b address this question by showing that the extended
1708 Ricker is capable of producing such multiple attractors (we show cases with one exclusion attractor
1709 and one coexistence attractor). Due to oscillations and a difference in the log-concavity of growth
1710 between species, traditional cases of bistability (Fig. 5a) and coexistence (Fig. 5b) are transformed into
1711 these novel competitive outcomes.

1712



1713

1714 **Figure 5:** Multiple attractors. (a) Dynamics of two competitors with growth functions given by
 1715 $G_i = \exp\{\ln(r_i)(1 - [(N_i(t) + c_{ij}N_j(t))/K_i]^{\gamma_i})\}$, where $r_1=5$, $r_2=2$, $K_1=K_2=10$, $\gamma_1=2$, $\gamma_2=1$, $c_{12}=c_{21}=1.1$. Note that
 1716 c_{ij} is the standard “competition coefficient” and that condition (3) may not be satisfied upon inclusion of
 1717 arbitrary coefficients (previously we have assumed $c_{ij}=c_{ji}=1$). Here the classical expectation from
 1718 isocline orientation is bistability, where one or the other species, but not both, can persist. Instead we
 1719 find coexistence (approaching a period-2 cycle) from the initial conditions given in white region and
 1720 exclusion of species 1 by species 2 from the initial conditions given by the blue region. Example
 1721 trajectories are shown to the right, corresponding to initial conditions given by the “x’s”. (b) The same
 1722 model with $r_1=7$, $r_2=80$, $K_1=K_2=10$, $\gamma_1=0.9$, $\gamma_2=0.5$, $c_{12}=c_{21}=0.9$. Here the classical expectation (from
 1723 isocline orientation) is coexistence. Instead we find coexistence (approaching a fixed point) from the
 1724 initial conditions given in white region and exclusion of species 1 by species 2 (approaching a period 2
 1725 cycle) from the initial conditions given by the blue region. Example trajectories are shown to the right,
 1726 corresponding to initial conditions given by the “x’s”.

1727 A second sample application of our framework involves the management of harvested species. Some
1728 species are managed so that harvesting only occurs once an abundance threshold is surpassed (Lande et
1729 al., 1997). If the managed species has a competitor and both species reproduce in discrete events, then
1730 it is theoretically possible that a management policy of this kind will actually drive the competitor of
1731 the managed species extinct. This can occur because the competitor may depend on existing
1732 fluctuations in the managed species. If harvesting has the effect of reducing these fluctuations (Lande
1733 et al., 1997), the competitor can permanently exit the system (Supplementary Information, Fig D4a).
1734 On the flip side, Anderson *et al.* (2008) have suggested that harvesting may *destabilize* populations,
1735 perhaps due to selection for altered intrinsic growth rates. In the Supplementary Information, we
1736 demonstrate that selection for a higher growth rate in one harvested species can drive a competitor
1737 extinct (Fig. D4c). These harvesting impacts can also have the reverse effect, allowing a previously
1738 excluded competitor to invade (Supplementary Information, Figs. D4b and D4d).

1739

1740 A third sample application of our framework shows that these same ideas are not restricted to
1741 ecological competition alone but apply to other species interactions. In epidemiology, the quantity R_0 is
1742 related to the rate of increase of a pathogen when extremely rare. If $R_0 < 1$, the disease declines to
1743 extinction. Generally, R_0 is evaluated at some equilibrium host abundance. However, if the host
1744 population (with a log-convex growth curve) reproduces discretely, then a disease can spread even
1745 when the equilibrium-based $R_0 < 1$ (Supplementary Information, Fig. D5a). Conversely, oscillations in a
1746 host (with a log-concave growth curve) could force the disease extinct even if the equilibrium-based
1747 $R_0 > 1$ (Supplementary Information, Fig. D5b). Thus, it is essential to consider host fluctuations when
1748 predicting the likelihood of an epidemic.

1749

1750 Beyond these sample applications, many species in nature exhibit discrete bursts of reproduction,
1751 frequently coincident with seasonal patterns (*e.g.*, annual plants and various insects). From the analysis
1752 of time-series data in natural and laboratory populations, and from evolutionary theoretical
1753 considerations, several authors have suggested that natural populations likely exhibit periodic and
1754 perhaps chaotic fluctuations (Anderson et al., 2008; Benincà et al., 2008; Edmunds et al., 2003;
1755 Ferriere and Gatto, 1993; Schaffer and Kot, 1986; Tilman and Wedin, 1991), although the subject has
1756 hardly been free from debate (Doebeli and Koella, 1996, 1995; Hassell et al., 1976; Lande et al., 1997).
1757 If endogenous fluctuations are possible, our analysis suggests that the shape (log-concavity) of growth
1758 functions will affect both the moments of a resident species as well as the way in which these moments
1759 are “felt” by an invader. In experimental or observational systems, empirical assessment of the shape
1760 of per capita growth curves in competitive, host-pathogen, and predator-prey systems will help
1761 determine whether such endogenous fluctuations can promote species diversity or even reverse
1762 expected outcomes in nature.

1763
1764 **Appendix A: Proof of the discrete-time competitive exclusion principle**

1765 Suppose that species k has the highest equilibrium when alone of S competing species in a Volterrian
1766 community. For any $i \neq k$, we define:

1767
$$\Omega_i(t) = \frac{N_i(t)^{1/\beta_i}}{N_k(t)^{1/\beta_k}}$$

1768 By equation (2), it follows that

1769
$$\Omega_i(t + 1) = \frac{G_i(\mathbf{N}(t))^{1/\beta_i}}{G_k(\mathbf{N}(t))^{1/\beta_k}} \Omega_i(t)$$

1770 By condition (3), $G_i(\mathbf{N}(t)) = \exp\{\alpha_i - \beta_i H(\mathbf{N}(t))\}$ and we have

1771
$$\Omega_i(t + 1) = e^{(\Phi_i - \Phi_k)} \Omega_i(t)$$

1772 where $\Phi_i = \alpha_i/\beta_i$. Letting $\eta_i = e^{(\Phi_i - \Phi_k)}$, we have the following solution for $\Omega_i(t)$:

1773
$$\Omega_i(t) = (\eta_i)^t \Omega_i(0)$$

1774 Since $\Phi_i < \Phi_k$ (see section B.5 of the Supplementary Information), we have $0 < \eta_i < 1$. Thus,

1775
$$\lim_{t \rightarrow \infty} \Omega_i(t) = \lim_{t \rightarrow \infty} (\eta_i)^t \Omega_i(0) = 0$$

1776 Each species has an upper bound (see section B.2 of the Supplementary Information). Let the upper
1777 bound of species k be given by N_k^{\max} . We must have

1778
$$0 \leq \frac{N_i(t)^{1/\beta_i}}{[N_k^{\max}]^{1/\beta_k}} \leq \frac{N_j(t)^{1/\beta_i}}{N_k(t)^{1/\beta_k}}$$

1779 Since $\lim_{t \rightarrow \infty} 0 = 0$ and $\lim_{t \rightarrow \infty} \frac{N_j(t)^{1/\beta_i}}{N_k(t)^{1/\beta_k}} = 0$, the squeeze rule for limits guarantees $\lim_{t \rightarrow \infty} \frac{N_i(t)^{1/\beta_i}}{[N_k^{\max}]^{1/\beta_k}} = 0$.

1780 Using the scalar rule for limits, it follows that $\lim_{t \rightarrow \infty} N_i(t)^{1/\beta_i} = 0$.

1781 Because $\beta_i > 0$ and $N_i(t) > 0$ for all t ,

1782
$$\lim_{t \rightarrow \infty} N_i(t) = 0$$

1783 This means all species other than species k go extinct. We now turn to species k .

1784

1785 Assume that species k also goes extinct, meaning $\lim_{t \rightarrow \infty} N_k(t) = 0$. Given that G_k is continuous and

1786 $G_k(\vec{\mathbf{0}}) > 1$, there exists some $\varepsilon > 0$, such that if $\|\mathbf{N}\| < \varepsilon$, $G_k(\mathbf{N}) > 1$. If $\lim_{t \rightarrow \infty} N_k(t) = 0$, then, at some time

1787 point t^* , $\mathbf{N}(t^*)$ will be located closer than ε to the origin and $\mathbf{N}(t)$ will stay closer to the origin than ε for

1788 all $t \geq t^*$. However, this means that $N_k(t+1) = G_k(\mathbf{N}(t))N_k(t) > N_k(t)$ for all $t \geq t^*$. Given that $N_k(t^*) > 0$, it

1789 cannot then be the case that $\lim_{t \rightarrow \infty} N_k(t) = 0$, which contradicts our assumption that species k goes

1790 extinct. Therefore, we may conclude that species k persists and all other species are driven to

1791 extinction, which completes the proof of the competitive exclusion principle.

1792

1793 Given some initial condition for a Volterrian community, we now show that it must be contained
 1794 within a shifting lower-dimensional subspace. To do this, we define:

$$1795 \quad \Lambda(t) = \left\{ \prod_{i=1}^S \frac{N_j(t)^{1/\beta_i}}{N_k(t)^{1/\beta_k}} \right\}^{1/S}$$

1796 By equation (2), we have the following:

$$1797 \quad \Lambda(t+1) = \left\{ \prod_{i=1}^S \frac{G_i(\mathbf{N}(t))^{1/\beta_i}}{G_k(\mathbf{N}(t))^{1/\beta_k}} \right\}^{1/S} \Lambda(t)$$

1798 Following the earlier approach starting from condition (3), this can be rewritten as

$$1799 \quad \Lambda(t+1) = e^{(\bar{\Phi}-\Phi_k)} \Lambda(t)$$

1800 where $\bar{\Phi} = \frac{1}{S} \sum_{i=1}^S \Phi_i$. Iterating gives us the general formula:

$$1801 \quad \Lambda(t) = \kappa^t \Lambda(0)$$

1802 with $\kappa = e^{(\bar{\Phi}-\Phi_k)}$. Using this relationship, we know that the community must be in a subspace at t
 1803 satisfying:

$$1804 \quad N_k = (\kappa^{-\omega_k})^t (\Lambda(0))^{-\omega_k} \prod_{i \in \mathbf{S}_{-k}} N_i^{\omega_k/S\beta_i}$$

1805 where $\omega_k = \beta_k S / (S - 1)$ and \mathbf{S}_{-k} is the set of integers from 1 to S without k . Here we take the density
 1806 of species k as the dependent variable. In Figure 3 and the Supplementary Information (section B.7) we
 1807 show how dynamics (in particular, competitive exclusion) can be visualized using this moving
 1808 subspace.

1809

1810 **Appendix B: Derivation of the invasion heuristic for 2-species communities**

1811 Consider two species, labeled 1 and 2. Species 1 will be the resident species. In the absence of species
 1812 2, the abundance of species 1 enters a bounded positive interval (given our assumptions about growth

1813 functions; see Supplementary Information, section A.3). Species 2 is the invader and starts at a very
 1814 low density (such that its initial success is determined by its growth function and the abundance of
 1815 species 1, but not its own abundance). The population recursion for the invader is given by:

$$1816 \quad N_2(t+1) = G_2(N_1(t), N_2(t))N_2(t)$$

1817 If an invader is to increase from very low density, then its long-term per capita growth rate (the
 1818 relevant Lyapunov number, \widetilde{G}_2) must be greater than unity. In other words:

$$1819 \quad \widetilde{G}_2 = \lim_{T \rightarrow \infty} \sqrt[T]{\prod_{t=0}^{T-1} G_2(N_1(t), 0)} > 1$$

1820 Alternatively, this can be expressed as:

$$1821 \quad \ln \widetilde{G}_2 = \lim_{T \rightarrow \infty} \left\{ \frac{1}{T} \sum_{t=0}^{T-1} \ln G_2(N_1(t), 0) \right\} > 0$$

1822 Given that the density of species 1 gets trapped in a bounded interval, the mean abundance and
 1823 variance in abundance of the resident are:

$$1824 \quad \overline{N}_1 = \lim_{T \rightarrow \infty} \left\{ \frac{1}{T} \sum_{t=0}^{T-1} N_1(t) \right\}$$

$$1825 \quad \sigma_{N_1}^2 = \lim_{T \rightarrow \infty} \left\{ \frac{1}{T} \sum_{t=0}^{T-1} (N_1(t) - \overline{N}_1)^2 \right\}$$

1826 assuming both limits exist. To estimate $\ln \widetilde{G}_2$, we use a second-order Taylor series approximation of
 1827 $\ln G_2(N_1(t), 0)$ centered at the mean resident abundance, \overline{N}_1 :

$$1828 \quad \ln \widetilde{G}_2 \approx \lim_{T \rightarrow \infty} \frac{1}{T} \sum_{t=0}^{T-1} \left\{ \ln G_2(\overline{N}_1, 0) + (N_1(t) - \overline{N}_1) \frac{d \ln G_2(N_1, 0)}{dN_1} \Big|_{N_1=\overline{N}_1} \right.$$

$$1829 \quad \left. + \left(\frac{(N_1(t) - \overline{N}_1)^2}{2} \right) \frac{d^2 \ln G_2(N_1, 0)}{dN_1^2} \Big|_{N_1=\overline{N}_1} \right\}$$

1830 By using the scalar and additive rules for limits, we have:

$$\begin{aligned}
 1831 \quad \ln \widetilde{G}_2 &\approx \ln G_2(\overline{N}_1, 0) + \left(\lim_{T \rightarrow \infty} \frac{1}{T} \sum_{t=0}^T N_1(t) \right) \frac{d \ln G_2(N_1, 0)}{dN_1} \Big|_{N_1=\overline{N}_1} - \overline{N}_1 \frac{d \ln G_2(N_1, 0)}{dN_1} \Big|_{N_1=\overline{N}_1} \\
 1832 \quad &+ \left(\lim_{T \rightarrow \infty} \frac{1}{T} \sum_{t=0}^T (N_1(t) - \overline{N}_1)^2 \right) \left(\frac{1}{2} \right) \frac{d^2 \ln G_2(N_1, 0)}{dN_1^2} \Big|_{N_1=\overline{N}_1}
 \end{aligned}$$

1833 Using the definitions of the mean and variance, we have:

$$1834 \quad \ln \widetilde{G}_2 \approx \ln G_2(\overline{N}_1, 0) + \left(\frac{\sigma_{N_1}^2}{2} \right) \frac{d^2 \ln G_2(N_1, 0)}{dN_1^2} \Big|_{N_1=\overline{N}_1}$$

1835 Or simply

$$1836 \quad \widetilde{G}_2 \approx G_2(\overline{N}_1, 0) \exp \left\{ \left(\frac{\sigma_{N_1}^2}{2} \right) \frac{d^2 \ln G_2(N_1, 0)}{dN_1^2} \Big|_{N_1=\overline{N}_1} \right\}$$

1837 This approximation derives from a second-order Taylor series. If the logarithm of the invader's growth
 1838 function ($\ln G_2$) is linear or quadratic, then the approximation is exact.

1839

1840

1841

1842

1843

1844

1845

1846

1847

1848

1849

1850

1851

1852

1853 **References**

1854

- 1855 Adler, F.R. (1990). Coexistence of two types on a single resource in discrete time. *J. Math. Biol.* 28,
1856 695–713.
- 1857 Anderson, C.N.K., Hsieh, C., Sandin, S.A., Hewitt, R., Hollowed, A., Beddington, J., May, R.M., and
1858 Sugihara, G. (2008). Why fishing magnifies fluctuations in fish abundance. *Nature* 452, 835–
1859 839.
- 1860 Armstrong, R.A., and McGehee, R. (1980). Competitive Exclusion. *The American Naturalist* 115,
1861 151–170.
- 1862 Asmussen, M.A. (1979). Regular and chaotic cycling in models of ecological genetics. *Theoretical*
1863 *Population Biology* 16, 172–190.
- 1864 Benincà, E., Huisman, J., Heerkloss, R., Jöhnk, K.D., Branco, P., Van Nes, E.H., Scheffer, M., and
1865 Ellner, S.P. (2008). Chaos in a long-term experiment with a plankton community. *Nature* 451,
1866 822–825.
- 1867 Chesson, P. (2000). Mechanisms of Maintenance of Species Diversity. *Annual Review of Ecology and*
1868 *Systematics* 31, 343–366.
- 1869 Cushing, J.M., Leverage, S., Chitnis, N., and Henson, S.M. (2004). Some Discrete Competition Models
1870 and the Competitive Exclusion Principle†. *Journal of Difference Equations and Applications*
1871 10, 1139–1151.
- 1872 Doebeli, M., and Koella, J. (1996). Chaos and evolution. *Trends in Ecology & Evolution* 11, 220.
- 1873 Doebeli, M., and Koella, J.C. (1995). Evolution of Simple Population Dynamics. *Proceedings of the*
1874 *Royal Society of London B: Biological Sciences* 260, 119–125.
- 1875 Edmunds, J., Cushing, J.M., Costantino, R.F., Henson, S.M., Dennis, B., and Desharnais, R.A. (2003).
1876 Park’s *Tribolium* competition experiments: a non-equilibrium species coexistence hypothesis.
1877 *Journal of Animal Ecology* 72, 703–712.
- 1878 Ferriere, R., and Gatto, M. (1993). Chaotic Population Dynamics can Result from Natural Selection.
1879 *Proceedings of the Royal Society of London B: Biological Sciences* 251, 33–38.
- 1880 Ferriere, R., and Gatto, M. (1995). Lyapunov Exponents and the Mathematics of Invasion in
1881 Oscillatory or Chaotic Populations. *Theoretical Population Biology* 48, 126–171.
- 1882 Franke, J.E., and Yakubu, A.-A. (1991). Mutual exclusion versus coexistence for discrete competitive
1883 systems. *J. Math. Biol.* 30, 161–168.
- 1884 Gatto, M. (1993). The Evolutionary Optimality of Oscillatory and Chaotic Dynamics in Simple
1885 Population Models. *Theoretical Population Biology* 43, 310–336.
- 1886 Gause, G.F. (1934). *The Struggle for Existence* (Baltimore: Williams and Wilkins).
- 1887 Hardin, G. (1960). The Competitive Exclusion Principle. *Science* 131, 1292–1297.
- 1888 Hassell, M.P. (1975). Density-Dependence in Single-Species Populations. *Journal of Animal Ecology*
1889 44, 283–295.
- 1890 Hassell, M.P., and Comins, H.N. (1976). Discrete time models for two-species competition.
1891 *Theoretical Population Biology* 9, 202–221.
- 1892 Hassell, M.P., Lawton, J.H., and May, R.M. (1976). Patterns of Dynamical Behaviour in Single-
1893 Species Populations. *Journal of Animal Ecology* 45, 471–486.
- 1894 Hastings, A., Hom, C.L., Ellner, S., Turchin, P., and Godfray, H.C.J. (1993). Chaos in Ecology: Is
1895 Mother Nature a Strange Attractor? *Annual Review of Ecology and Systematics* 24, 1–33.
- 1896 Huisman, J., and Weissing, F.J. (1999). Biodiversity of plankton by species oscillations and chaos.
1897 *Nature* 402, 407–410.

- 1898 Lande, R., Sæther, B.-E., and Engen, S. (1997). Threshold Harvesting for Sustainability of Fluctuating
1899 Resources. *Ecology* 78, 1341–1350.
- 1900 Leslie, P.H., Park, T., and Mertz, D.B. (1968). The Effect of Varying the Initial Numbers on the
1901 Outcome of Competition Between Two Tribolium Species. *Journal of Animal Ecology* 37, 9–
1902 23.
- 1903 May, R.M. (1974). Biological Populations with Nonoverlapping Generations: Stable Points, Stable
1904 Cycles, and Chaos. *Science* 186, 645–647.
- 1905 May, R.M. (1975). Biological populations obeying difference equations: Stable points, stable cycles,
1906 and chaos. *Journal of Theoretical Biology* 51, 511–524.
- 1907 May, R.M., and Oster, G.F. (1976). Bifurcations and Dynamic Complexity in Simple Ecological
1908 Models. *The American Naturalist* 110, 573–599.
- 1909 Metz, J.A., Nisbet, R.M., and Geritz, S.A. (1992). How should we define “fitness” for general
1910 ecological scenarios? *Trends Ecol. Evol. (Amst.)* 7, 198–202.
- 1911 Nelder, J.A. (1961). The Fitting of a Generalization of the Logistic Curve. *Biometrics* 17, 89–110.
- 1912 Ricker, W.E. (1954). Stock and Recruitment. *J Fisheries Research Board of Canada* 11, 559–623.
- 1913 Schaffer, W.M., and Kot, M. (1986). Chaos in ecological systems: The coals that Newcastle forgot.
1914 *Trends in Ecology & Evolution* 1, 58–63.
- 1915 Tilman, D. (1982). *Resource Competition and Community Structure* (Princeton University Press).
- 1916 Tilman, D., and Wedin, D. (1991). Oscillations and chaos in the dynamics of a perennial grass. *Nature*
1917 353, 653–655.
- 1918 Vandermeer, J., Evans, M.A., Foster, P., Höök, T., Reiskind, M., and Wund, M. (2002). Increased
1919 competition may promote species coexistence. *PNAS* 99, 8731–8736.
- 1920 Volterra, V. (1928). Variations and Fluctuations of the Number of Individuals in Animal Species living
1921 together. *J. Cons. Int. Explor. Mer* 3, 3–51.
- 1922
- 1923